Fed-batch growth of *Rhizopus oryzae*: eliminating ethanol formation by controlling glucose addition

Nicolaas Willem de Jongh

CVD 800

2021-05-30

Fed-batch growth of *Rhizopus oryzae*: eliminating ethanol formation by controlling glucose addition

Nicolaas Willem de Jongh
13276702

Department of Chemical Engineering
University of Pretoria

CVD 800

2021-05-30

Fed-batch growth of *Rhizopus oryzae*: eliminating ethanol formation by controlling glucose addition

Abstract

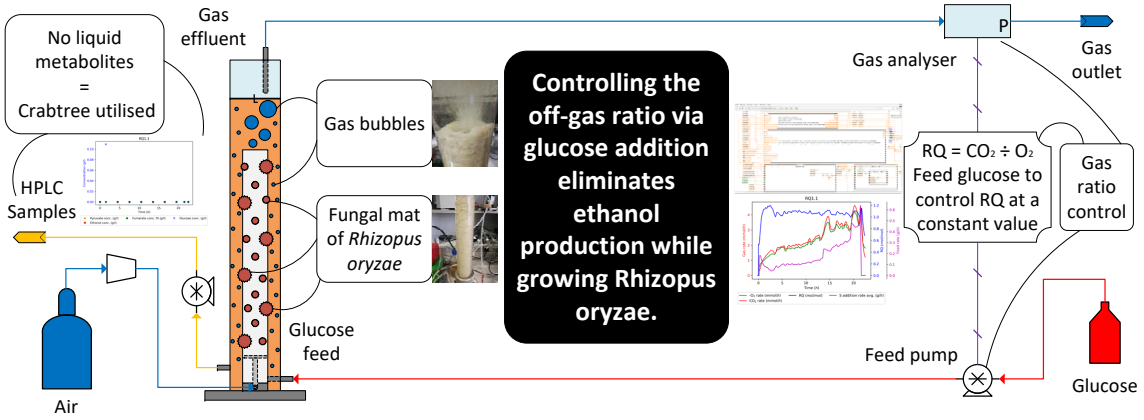

Rhizopus oryzae is a prominent strain for producing fumarate, where biomass growth precedes fumarate production. The natural biofilm growth of *R. oryzae* as fungal mat was investigated using different glucose addition strategies in a novel fed-batch fermenter. Batch growth was compared through three fed-batch runs, each with a different glucose addition strategy. The fed-batch runs involved a constant glucose feed (CGF) of 0.075 $g\,h^{-1}$ and controlled glucose feeds in order to keep the respiration quotient (RQ) at either 1.3 mol CO_2 mol^{-1} O_2 (RQ1.3) or 1.1 mol CO_2 mol^{-1} O_2 (RQ1.1). Ethanol overflow via the established Crabtree mechanism was completely negated for the CGF and RQ1.1 runs, while the batch and RQ1.3 runs exhibited significant ethanol formation. Biomass yield on glucose was found to be 0.476 $g\,g^{-1}$ (RQ1.1), 0.194 $g\,g^{-1}$ (RQ1.3), 0.125 $g\,g^{-1}$ (CGF) and 0.144 $g\,g^{-1}$ (batch). The results indicate a three-fold improvement in biomass yield when comparing the batch run with the RQ1.1 run. In addition, the RQ1.1 run resulted in zero detectable byproducts, unlike the batch scenario where pyruvate and fumarate were associated with ethanol formation. Clear evidence is provided that glucose overflow can be fully eliminated during *R. oryzae* growth, significantly affecting the biomass yield on glucose.

Keywords: *Rhizopus oryzae*, respiration quotient, controlled substrate addition, Crabtree effect, fumarate production, fed-batch reactor

Acknowledgements

This work was supported by the University of Pretoria and by the CSIR Inter-bursary Programme, South Africa. Opinions expressed are those of the author and not necessarily attributed to the funding sources. The funding sources were not involved in the study, or in the design, in the collection, analysis and interpretation of data in the writing of any associated articles and reports, or in the writing of this dissertation.

Gratitude is expressed towards Prof. Willie Nicol for general research guidance and his role as supervisor. Aside from being very knowledgeable in the bioreaction field, his inputs throughout this study were very professional, practical and inspiring.

The hard work and personal sacrifice of everyone in the Bioreaction Engineering Research Group at the University of Pretoria is acknowledged, especially that of Reuben Swart.

My parents, Hans de Jongh and Lizanda Wessels, are thanked for their financial and emotional support during the past number of years; without them, neither this study nor my tertiary education would have been possible.

Martie Peens is especially appreciated for her support and companionship during our spiritual and relational journey of growth over the past number of years, helping to make this study possible.

Contents

List of Figures

List of Tables

Nomenclature

Constants

K	Gas rate conversion factor	$2\,373 \times 10^{-3}$ mol min ml^{-1} h^{-1}
V_g	Reactor gas volume	0 3 l
V_l	Rector liquid volume	1 l
$y_{O_2}^{air}$	Reactor air feed O_2 mole fraction	0 21 i

Variables

$\vec{c}$	System specification vector	cmol l^{-1} h^{-1}
$\vec{r}$	Calculated rates vector	cmol l^{-1} h^{-1}
c_i^f	Component feed liquid concentration	cmol l^{-1}
$c_i l$	Component reactor liquid concentration	cmol l^{-1}
D	Dilution rate	h^{-1}
e	Set point-measurement error	i
$e_{CO_2\ spec}^{relative}$	Relative error between measured and CO_2 calculated final biomass mass	i
$e_{O_2\ spec}^{relative}$	Relative error between measured and O_2 calculated final biomass mass	i
I_{term}	Accumulative integral term	s
I_{term}^{t-1}	Accumulative integral term at previous time-step	s
K_P	Proportional gain constant	cmol l^{-1} h^{-1}
$m_S^{predicted}$	Predicted accumulated glucose mass fed	g
$m_X^{calc,CO_2\ spec}$	Calculated final biomass mass using the CO_2 specification	g
$m_X^{calc,O_2\ spec}$	Calculated final biomass mass using the O_2 specification	g
$m_X^{mesured\ final}$	Measured final biomass mass	g
$m_X^{predicted}$	Predicted final biomass mass	g
P_X	Biomass productivity	mg l^{-1} h^{-1}
Q_{air}^f	Reactor air feed rate	ml min^{-1}

$Q^f_{CO_2}$	Reactor CO_2 feed rate	$\mathrm{ml\,min^{-1}}$
Q^f_{liq}	Total reactor liquid feed rate	$\mathrm{l\,h^{-1}}$
Q^f_{tot}	Reactor total gas feed rate	$\mathrm{ml\,min^{-1}}$
r_C	CO_2 rate	$\mathrm{cmol\,l^{-1}\,h^{-1}}$
r^E_C	CO_2 production rate due to ethanol production	$\mathrm{mol\,l^{-1}\,h^{-1}}$
r^{FA}_C	CO_2 consumption rate due to fumaric acid production	$\mathrm{mol\,l^{-1}\,h^{-1}}$
r^{tot}_C	Total CO_2 production rate	$\mathrm{mol\,l^{-1}\,h^{-1}}$
$r^{X+resp,estimate}_C$	Estimated CO_2 production rate due to only respiration and biomass formation	$\mathrm{mol\,l^{-1}\,h^{-1}}$
r^{X+resp}_C	CO_2 production rate due to only respiration and biomass formation	$\mathrm{mol\,l^{-1}\,h^{-1}}$
r_E	Ethanol rate	$\mathrm{cmol\,l^{-1}\,h^{-1}}$
r_G	Glycerol rate	$\mathrm{cmol\,l^{-1}\,h^{-1}}$
r_i	Component reaction rate	$\mathrm{cmol\,l^{-1}\,h^{-1}}$
r^{calc}_i	Calculated component rate	$\mathrm{cmol\,l^{-1}\,h^{-1}}$
r^{meas}_i	Measured component rate	$\mathrm{cmol\,l^{-1}\,h^{-1}}$
r_O	O_2 rate	$\mathrm{cmol\,l^{-1}\,h^{-1}}$
r^{tot}_O	Total O_2 consumption rate	$\mathrm{mol\,l^{-1}\,h^{-1}}$
r_S	Glucose rate	$\mathrm{cmol\,l^{-1}\,h^{-1}}$
$r^{fitted\ feed\ rate}_S$	Fitted glucose feed rate correlation	$\mathrm{cmol\,l^{-1}\,h^{-1}}$
r^f_S	Glucose feed rate	$\mathrm{cmol\,l^{-1}\,h^{-1}}$
$r^{liq\ met}_S$	Liquid metabolite producing glucose consumption rate	$\mathrm{cmol\,l^{-1}\,h^{-1}}$
r^{net}_S	Net glucose consumption rate	$\mathrm{cmol\,l^{-1}\,h^{-1}}$
r^{tot}_S	Total glucose consumption rate	$\mathrm{cmol\,l^{-1}\,h^{-1}}$
r_U	Urea rate	$\mathrm{cmol\,l^{-1}\,h^{-1}}$
r_W	Water rate	$\mathrm{cmol\,l^{-1}\,h^{-1}}$
r_X	Biomass rate	$\mathrm{cmol\,l^{-1}\,h^{-1}}$

r_{FA}	Fumaric acid rate	$\mathrm{cmol\,l^{-1}\,h^{-1}}$
r_{LA}	Lactic acid rate	$\mathrm{cmol\,l^{-1}\,h^{-1}}$
r_{MA}	Malic acid rate	$\mathrm{cmol\,l^{-1}\,h^{-1}}$
r_{PA}	Pyruvic acid rate	$\mathrm{cmol\,l^{-1}\,h^{-1}}$
r_{SA}	Succinic acid rate	$\mathrm{cmol\,l^{-1}\,h^{-1}}$
RQ	Respiration quotient	i
$RQ^{desired}$	Desired respiration quotient	i
RQ_{avg}	Average respiration quotient	i
RQ_{meas}	Measured respiration quotient	i
S	Metabolic coefficient matrix	$\mathrm{cmol\,l^{-1}\,h^{-1}}$
SP	Set point	i
t	Time	h
T_I	Integral time constant	s
y_{CO_2}	Effluent gas measured CO_2 mole fraction	i
$y_{CO_2}^{baseline}$	Effluent gas measured CO_2 mole fraction at steady state before inoculation	i
$y_{CO_2}^{cal}$	Effluent gas calibrated CO_2 mole fraction	i
y_{O_2}	Effluent gas measured O_2 mole fraction	i
$y_{O_2}^{baseline}$	Effluent gas measured O_2 mole fraction at steady state before inoculation	i
$y_{O_2}^{cal}$	Effluent gas calibrated O_2 mole fraction	i
$Y_{SX}^{predicted}$	Predicted yield of biomass produced on glucose consumed	i

Abbreviations

ADH alcohol dehydrogenase

ATCC American Type Culture Collection

CGF constant glucose feed addition fed-batch experiment

CSIR Council for Scientific and Industrial Research

HPLC high-performance liquid chromatography

MRM metabolic regime map

PI proportional-integral

R^2 coefficient of determination

RI refractive index

RQ respiration quotient

RQ1.1 fed-batch experiment with RQ kept at 1.1

RQ1.3 fed-batch experiment with RQ kept at 1.3

RSD relative standard deviation

SCDA short-chain dicarboxylic acid

TCA tricarboxylic acid

1 Introduction

The dicarboxylic acids of the tricarboxylic acid (TCA) cycle, namely malate, fumarate and succinate, are important biobased intermediates for the production of various bulk-scale chemicals (Werpy & Petersen, 2004). Malate, fumarate and succinate are very close structurally. Of these three, fumarate is the most chemically diverse due to its double bond, easily producing malate or succinate. Dehydration of fumarate also produces maleic anhydride, with a significant market size of approximately 4.36 billion USD (projected 2025 market size) (Grand View Research, 2019). Fumaric acid also has a very low solubility in water (4.3 $g\,l^{-1}$ at 15 °C) (Bélafi-Bakó, Nemestóthy & Gubicza, 2004) which significantly simplifies downstream processing from the fermenter.

Fumarate itself is widely used in industry. It is used in the treatment of medical conditions (Mrowietz, Christophers & Altmeyer, 1999; Schimrigk *et al*, 2006) and as a feed additive for animals (Lan & Kim, 2018; Patten & Waldroup, 1988; Beauchemin & McGinn, 2006) to improve their metabolic processes. Fumaric acid is used as a food acidulant (Shukla, 2017) and in baking soda (Cepeda *et al*, 2000). Industrial production of polyester resins also utilises fumarate as feedstock (Rokicki & Wodzicki, 2000). Doscher *et al* (1941) also discusses applications of fumarate in the production of synthetic resins, coating compounds and plasticisers (Doscher *et al*, 1941).

The biological production of fumaric acid is mostly associated with the *Rhizopus* fungal genus. *Escherichia coli* has been manipulated to produce fumarate in small quantities (Song *et al*, 2013), but the results are far from those obtained in prominent *Rhizopus* fermentations. *Rhizopus oryzae* (ATCC 20344, also referred to as *Rhizopus delemar* (Abe *et al*, 2007)) is one of the most prominent and studied *Rhizopus* species for producing fumarate, with the titres obtained being between 25 $g\,l^{-1}$ (B Zhang, Skory & Yang, 2012) and 103 $g\,l^{-1}$ (Rhodes *et al*, 1962) and the productivities between 0.19 $g\,l^{-1}\,h^{-1}$ (Roa Engel, Van Gulik, *et al*, 2011) and 1.21 $g\,l^{-1}\,h^{-1}$ (Das, Brar & Verma, 2015). Genetic modifications of *R. oryzae* have been proved to result in minor fermentation improvements (B Zhang, Skory, *et al*, 2012). The paper by Sebastian et al. (Sebastian *et al*, 2019) is a useful reference for comparative fumarate fermentations.

Depending on the desired product, different medium compositions and reactor setups are utilised when fermenting with *R. oryzae*. Examples include introducing plant hormones into a whey medium for enhanced growth and chitosan production (Chatterjee *et al*, 2008), and utilising *R. oryzae* cells immobilised within biomass support particles as a whole-cell biocatalyst for the production of biodiesel fuel from plant oils (Ban *et al*, 2001). For targeted fumarate production, ethanol coproduction presents one of the most prominent challenges (Ghosh & Rani Ray, 2011); other challenges include appropriate

fermenter design and product inhibition effects. Ethanol as byproduct increases downstream separation costs and wastes valuable feedstock materials by decreasing the yield. Numerous strategies have been employed to minimise ethanol coproduction, such as mutation and the selection of strains with less-active ethanol-producing metabolic pathways (Bai, Zhao, *et al*, 2004; Fu *et al*, 2010) and overexpressing native mitochondrial fumarase (B Zhang & Yang, 2012). Oxygen availability plays a major role in the wastewater treatment process, where airlift bioreactors (Sepehri, Sarrafzadeh & Avateffazeli, 2020) and membrane bioreactors (Sepehri & Sarrafzadeh, 2018) may be used for uniform aeration and the filtration of oxygen-consuming heterotrophic bacteria, respectively. Similarly, ethanol production by *R. oryzae* is conventionally viewed as a result of insufficient availability of oxygen during fermentation. Numerous studies have attempted to increase the availability of cell oxygen by inducing biomass pelletisation in flasks, stirred tank reactors and airlift bioreactors (Bai, Jia, *et al*, 2003; Liao, Liu & Chen, 2007; Zhou, Du & Tsao, 2000; Yin *et al*, 1998; Maneeboon *et al*, 2010). Mycelial cotton-like floc formation (Park, Kosakai & Okabe, 1998) using a woven towel (Chotisubha-Anandha *et al*, 2011) and a honeycomb matrix (Wang *et al*, 2010) as growth scaffolding, as well as vigorous shaking during solid state fermentation also increases the cellular surface area for oxygen uptake. However, none of these attempts at improving oxygen availability have resulted in the elimination of ethanol coproduction. In a recent paper by Swart *et al* (2020) it was clearly shown that *R. oryzae* is a Crabtree-positive organism. This implies that ethanol production is a result of an overflow mechanism by which excessive glucose uptake is channelled into ethanol. The work showed that ethanol production can be completely avoided by manipulating the glucose availability in the fermenter.

The study by Swart *et al* (2020) employed the fermenter design developed by Naude & Nicol (2017), Naude & Nicol (2018a), and Naude & Nicol (2018b). In this fermenter biomass is naturally immobilised on both sides of a polypropylene tube, utilising shear force generated by the liquid recycle flowrate. The medium was agitated by high flowrate recycling of the fermentation broth from the inside to the outside of the polypropylene growth scaffold, and by alternating the flow direction every 2 min to prevent biomass tube clogging. The thickness of the attached fungal mat is controlled by the amount of glucose supplied for the growth part of the fermentation. The immobilised biomass enables fast replacement of the fermentation medium without removing any biomass. During this process the spent growth medium can be replaced with a nitrogen-lean production medium so that fumarate excretion is the major metabolic flux. The setup is also supplied with an off-gas analyser of oxygen and carbon dioxide that enables real-time analysis of fermentation fluxes. Most of the studies on this fermenter have focused on the fumarate production phase, where a nitrogen-lean medium is employed to enforce fumarate excretion (Naude & Nicol, 2017; Naude & Nicol, 2018a; Naude & Nicol, 2018b;

Swart *et al*, 2020).

The current study focused only on the growth phase of the fumarate fermentation. The objective was to maximise the yield of biomass on glucose by eliminating byproducts other than respiratory carbon dioxide. The paper by Swart *et al* (2020) has clearly proved that *R. oryzae* is a Crabtree-positive organism similar to *Saccharomyces cerevisiae* (Deken, 1966). Production of *S. cerevisiae* biomass is commonly associated with the control of glucose availability. The strategy employed is to manipulate the cellular uptake of glucose and to eliminate the aerobic formation of ethanol. Ethanol formation in Crabtree-positive organisms is a result of the glucose uptake rate which exceeds the glucose flux that can be processed by the mitochondria of the eukariotic cell (Swart *et al*, 2020). The surplus of intracellular glucose is accordingly channelled to ethanol (often described as an overflow) whereby additional cellular energy is obtained (Deken, 1966). To avoid ethanol overflow a fed-batch fermenter is employed where the feed rate is adjusted as the biomass content in the fermenter increases. The objective of the glucose feeding is to maintain a cellular glucose uptake rate less than or equal to the glucose flux that the respiration system can process (XC Zhang *et al*, 1994; Woehrer & Roehr, 1981). Overfeeding of glucose results in the formation of ethanol; this can be observed in the off-gas product, with an increase in carbon dioxide content due to its coformation with ethanol (Dantigny *et al*, 2005).

The concept of ethanol-free biomass production for *R. oryzae* was investigated. A batch fermentation with excess glucose provides the baseline for improving the growth yield on glucose. Subsequently, various fed-batch strategies were employed in order to reduce the formation of ethanol and other byproducts. The first fed-batch run employed a constant glucose feed (CGF), while the other runs used the off-gas ratio of carbon dioxide to oxygen (respiration quotient or RQ) to alter the glucose feed during the fermentation. Two different setpoint values of RQ were investigated.

2 Theory

2.1 Industry

The double polarity of short chain dicarboxylic acids (SCDAs) makes them important intermediates in the production of bulk-scale chemicals. Many commercial materials are produced downstream from SCDAs due to their double polarity (Werpy & Petersen, 2004). Since the first oil crisis in the 1970s, plant and microbial SCDA sources have been explored as sustainable alternatives to traditional fossil feedstocks. Many microorganisms produce SCDAs. These form part of their cellular metabolic tricarboxylic acid (TCA) cycle functioning in the mitochondria. Economic interest lies predominantly in the form of three C4 molecules: malate, fumarate and succinate (Werpy & Petersen, 2004).

These three acids are structurally similar, with malate and succinate, respectively, being only a hydration and hydrogenation step away from fumarate. Due to its double bond, fumarate is the most diverse intermediate of the three, as it is more economically feasible to add chemically, rather than remove, H_2 and H_2O. In addition, fumarate is a single dehydration reaction away from maleic anhydride, which had a market size of 2.77 billion USD in 2018, a projected market size of 3.15 billion USD in 2020, and has a projected market size of 4.36 billion USD in 2025 (Grand View Research, 2019). The low fumaric acid solubility of 4.3 $\mathrm{g\,l^{-1}}$ at 15 °C (Bélafi-Bakó *et al*, 2004) renders the process objective of high product titre much less important than product yield and reaction productivity. The chemical structures of maleic acid, maleic anhydride and fumaric acid are presented in Figure 1 (Wojcieszak *et al*, 2015).

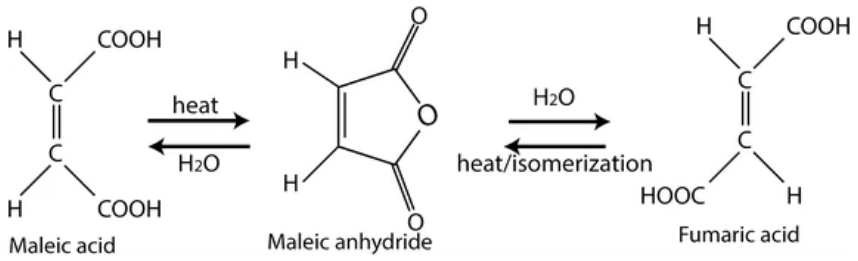

Figure 1: Chemical structures of maleic acid, maleic anhydride and fumaric acid (Wojcieszak *et al*, 2015).

2.2 Fumaric acid

Fumarate has a vast range of applications. It is used in the treatment of psoriasis (Mrowietz *et al*, 1999) and multiple sclerosis (Schimrigk *et al*, 2006). Piglets (Lan & Kim, 2018),

broilers (Patten & Waldroup, 1988) and cattle (Beauchemin & McGinn, 2006) are fed fumarate to reduce emissions of greenhouse-associated methane. Fumaric acid tastes more acidic than citric acid on a mass basis (1.36 g of citric acid to every 0.91 g of fumaric acid) and is suitable for use as a food acidulant (Shukla, 2017); it is also used as solid-state acid in baking soda (Cepeda *et al*, 2000). A high degree of cross-linking results when fumarate is utilised in the industrial production of polyester resins (Rokicki & Wodzicki, 2000). Fumarate has been shown to produce small pore sizes in the production of metal-organic frameworks for advanced electrochemical energy storage devices (Baumann *et al*, 2019). It is used to separate zirconium from aluminium, beryllium, uranium, nickel, barium, calcium, iron, manganese, thorium and the ceria earths in a single precipitation, and vanadium, chromium, titanium, and tin are completely removed in a double precipitation (Venkataramaniah & Raghava Rao, 1951). Other industrial fumarate applications are also discussed by Doscher et al (Doscher *et al*, 1941).

The name of fumaric acid is derived from the plant from which it was first isolated, *Fumaria officinalis* (family: Papaveraceae) (Roa Engel, Straathof, *et al*, 2008). The genus *Arabidopsis* in the Brassicaceae (cabbage and mustard) family is known to contain and utilize fumarate as possible carbon transporter (Chia *et al*, 2000). Plant-based fumarate production presents challenges regarding product consistency, low productivity and yield, and agricultural factors. The auxotrophic nature of SCDA-producing bacteria demands costly essential amino acids and vitamins for sustainable cultivation, which are typically available from complex sources such as yeast extract and corn steep liquor. These expensive sources complicate physiological understanding of the organism, retarding research and the progression of industrial applications. Although not a naturally high yield producer, *Escherichia coli* has been manipulated to produce fumarate efficiently (Song *et al*, 2013), despite the challenges associated with bacterial fumarate production. Eukaryotes such as fungi are able to utilise low-cost inorganic salts or simple organic compounds such as urea as sole nitrogen source, thereby presenting a direct advantage over bacteria as suitable biocatalysts for SCDA production.

2.3 *Rhizopus oryzae*

2.3.1 Biocatalyst selection

Numerous wild-type microorganisms have proved capable of producing fumarate, but few on an economically viable, industrial scale. *Rhizopus nigricans* was the first microorganism discovered that was able to produce fumaric acid (Foster & Waksman, 1939). In recent times, the genus *Rhizopus* has had great success in providing fumarate-producing

strains for the scientific community. *R. oryzae* especially stands out amongst other microorganisms for its simple nutritional requirements and high productivity (Das, Brar & Verma, 2016). Two main types of *R. oryzae* are commonly referred to: the lactate- and fumarate/malate-producing variants, respectively. It is proposed by Abe et al. (Abe *et al*, 2007) to refer to all fumarate/malate-producing variants as *Rhizopus delemar* and to all lactate-producing variants as *R. oryzae*. The strain ATCC 20344 has been extensively researched, especially regarding morphology studies (Liao, Liu & Chen, 2007) and high fumarate titre (Liao, Liu, Frear, *et al*, 2008). This strain has traditionally been referred to as *R. oryzae* (Deng & Aita, 2018; Liao, Liu, Frear, *et al*, 2008), but recently also as *R. delemar* (Odoni *et al*, 2017).

Although *R. oryzae* currently serves as the most promising fumarate producer, genetically manipulated mutants of *R. oryzae* have potential to compete with the natural organism, as they can operate predictably in specific conditions. However, when genetically altering a native producer, the organism is modified towards a specific objective in one specific medium and loses some of its robustness when a different production objective, such as biomass or malate production, is desired or when its media is altered significantly. Other than fumarate, *R. oryzae* may be used in the production of enzymes of immense industrial importance, namely lactic acid, ethanol, biodiesel and dry mycelium as flavour ester catalyst (Ghosh & Rani Ray, 2011).

Illustrated in Figure 2a are various growth morphologies of *R. oryzae* (Ilica *et al*, 2019); and a photo of *R. oryzae* cultured on potato dextrose agar is shown in Figure 2b.

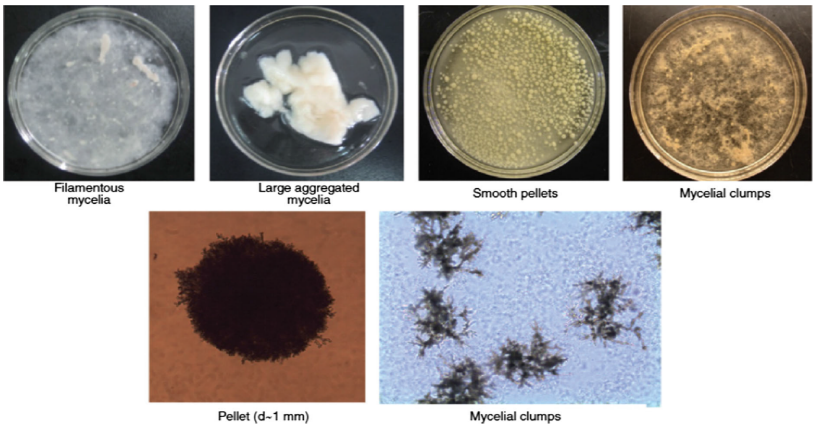

(a)

(b)

Figure 2: Various growth morphologies of *R. oryzae* (Ilica *et al*, 2019) (a); and *R. oryzae* fungal mat cultured on potato dextrose agar (b).

2.3.2 Organism metabolic map

The main carbon metabolism for *R. oryzae* is given in Figure 3 (Naude & Nicol, 2017).

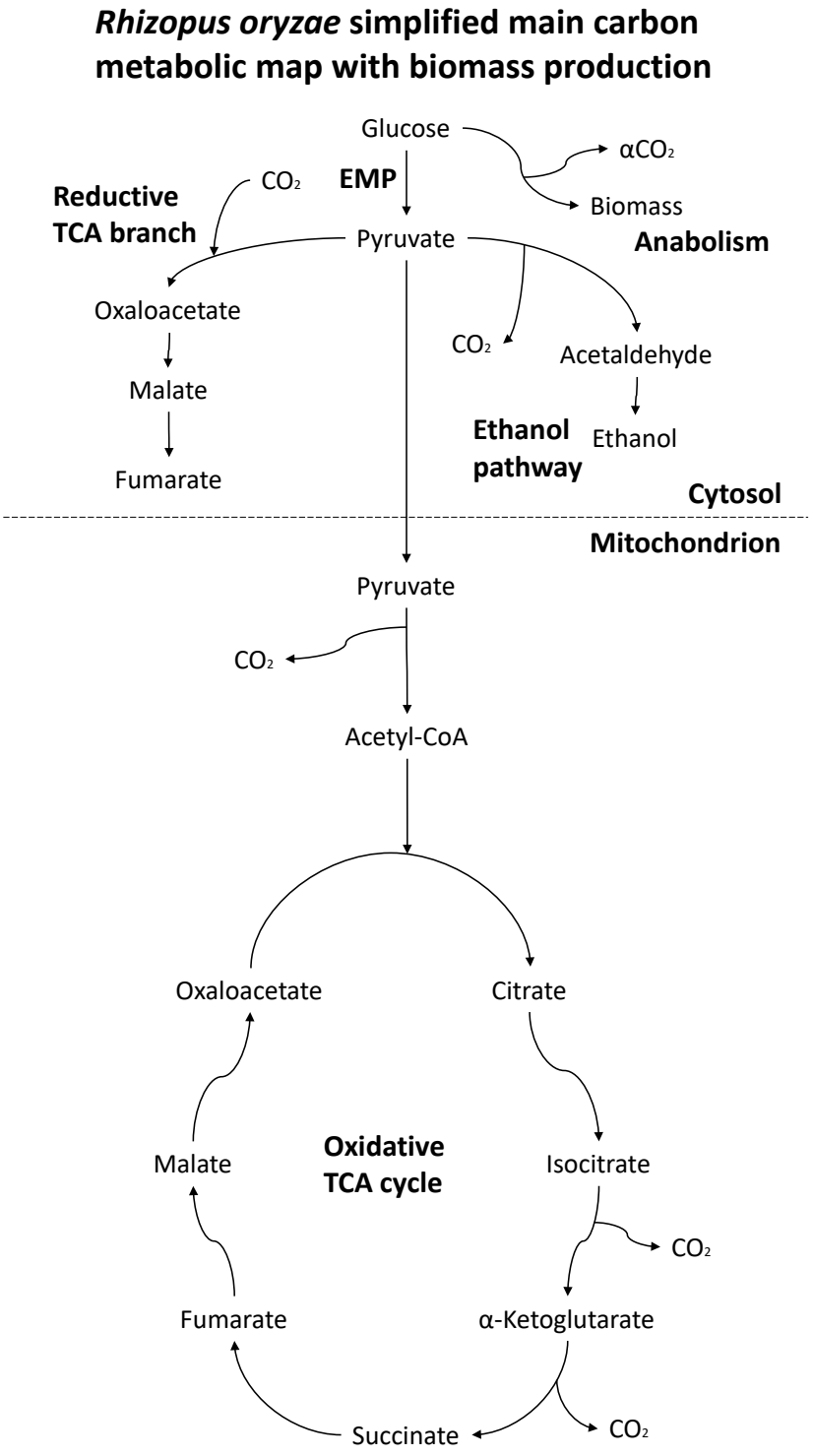

Figure 3: *Rhizopus oryzae* simplified main carbon metabolic map with biomass production (Naude & Nicol, 2017).

This metabolic process may be mathematically described by performing a mass balance over the system with the following overall reaction taking place:

$$
\begin{aligned}
(r_S)Glucose + (r_U)Urea + (r_O)Dioxygen \rightarrow (r_X)Biomass + (r_G)Glycerol \\
+(r_E)Ethanol + (r_{FA})Fumarate + (r_{SA})Succinate + (r_{MA})Malate \\
+(r_{PA})Pyruvate + (r_{LA})Lactate + (r_C)Carbon\ dioxide + (r_W)Water
\end{aligned} \tag{1}
$$

with each respective r_i denoting the volumetric reaction rate of the corresponding compound in $\mathrm{cmol\,l^{-1}\,h^{-1}}$. If all liquid catabolite and glucose concentrations as well as either one of the O_2 or CO_2 effluent gas concentrations are known, the system of equations may be solved for by including mol balances for C, H, O and N. This set of equations may be expressed as:

$$
\begin{pmatrix}
1 & 1 & 0 & 1 & 1 & 1 & 1 & 1 & 1 & 1 & 1 & 1 & 0 \\
2 & 4 & 0 & 1.8 & 8/3 & 3 & 1 & 3/2 & 3/2 & 4/3 & 2 & 0 & 2 \\
1 & 1 & 2 & 0.5 & 1 & 1/2 & 1 & 1 & 5/4 & 1 & 1 & 2 & 1 \\
0 & 2 & 0 & 0.16 & 0 & 0 & 0 & 0 & 0 & 0 & 0 & 0 & 0 \\
1 & 0 & 0 & 0 & 0 & 0 & 0 & 0 & 0 & 0 & 0 & 0 & 0 \\
0 & 0 & 1 & 0 & 0 & 0 & 0 & 0 & 0 & 0 & 0 & 0 & 0 \\
0 & 0 & 0 & 0 & 1 & 0 & 0 & 0 & 0 & 0 & 0 & 0 & 0 \\
0 & 0 & 0 & 0 & 0 & 1 & 0 & 0 & 0 & 0 & 0 & 0 & 0 \\
0 & 0 & 0 & 0 & 0 & 0 & 1 & 0 & 0 & 0 & 0 & 0 & 0 \\
0 & 0 & 0 & 0 & 0 & 0 & 0 & 1 & 0 & 0 & 0 & 0 & 0 \\
0 & 0 & 0 & 0 & 0 & 0 & 0 & 0 & 1 & 0 & 0 & 0 & 0 \\
0 & 0 & 0 & 0 & 0 & 0 & 0 & 0 & 0 & 1 & 0 & 0 & 0 \\
0 & 0 & 0 & 0 & 0 & 0 & 0 & 0 & 0 & 0 & 1 & 0 & 0
\end{pmatrix}
\begin{pmatrix}
r_S^{calc} \\ r_U^{calc} \\ r_O^{calc} \\ r_X^{calc} \\ r_G^{calc} \\ r_E^{calc} \\ r_{FA}^{calc} \\ r_{SA}^{calc} \\ r_{MA}^{calc} \\ r_{PA}^{calc} \\ r_{LA}^{calc} \\ r_C^{calc} \\ r_W^{calc}
\end{pmatrix}
=
\begin{pmatrix}
0 \\ 0 \\ 0 \\ 0 \\ r_S^{meas} \\ r_O^{meas} \\ r_G^{meas} \\ r_E^{meas} \\ r_{FA}^{meas} \\ r_{SA}^{meas} \\ r_{MA}^{meas} \\ r_{PA}^{meas} \\ r_{LA}^{meas}
\end{pmatrix}
$$

which may be simplified to:

$$
S\vec{r} = \vec{c} \tag{2}
$$

where $\vec{S}$ is the metabolic mass balance coefficient matrix, $\vec{r}$ is the calculated rates vector in $\mathrm{cmol\,l^{-1}\,h^{-1}}$ and $\vec{c}$ is the system specification vector in $\mathrm{cmol\,l^{-1}\,h^{-1}}$. The rates for all compounds are calculated at each time-step by solving for $\vec{r}$:

$$
\vec{r} = S^{-1}\vec{c} \tag{3}
$$

which provides the rate and therefore the concentration profile values for all metabolites (including biomass) over the duration of the experiment.

Depending on the desired product, different medium compositions and reactor setups are utilised when fermenting with *R. oryzae*. Examples of this are introducing plant hormones into a whey medium to enhance growth and chitosan production (Chatterjee *et al*, 2008), and utilising biomass support particles for the production of biodiesel from plant oils

(Ban *et al*, 2001). When fumarate or lactate production is desired the most common and prominent challenge encountered is how to eliminate simultaneous ethanol production. Ethanol, which is produced alongside the desired acid, increases downstream separation costs and wastes valuable feedstock materials. Numerous strategies have been employed to force acid yield improvement (thus eliminating the ethanol production) during fermentation, such as mutation and selection of strains with less active ethanol-producing metabolic pathways (Bai, Zhao, *et al*, 2004; Fu *et al*, 2010), and overexpressing native mitochondrial fumarase (B Zhang & Yang, 2012). Ethanol production is conventionally viewed as a result of insufficient oxygen availability during fermentation, resulting in many research studies attempting to increase cell oxygen availability by inducing biomass pelletisation in flasks, stirred tank reactors and airlift bioreactors (Bai, Jia, *et al*, 2003; Liao, Liu & Chen, 2007; Zhou *et al*, 2000; Yin *et al*, 1998; Maneeboon *et al*, 2010); mycelial cotton-like floc formation (Park *et al*, 1998), using a woven towel (Chotisubha-Anandha *et al*, 2011) and a honeycomb matrix (Wang *et al*, 2010) for growth scaffolding, as well as vigorous shaking during solid state fermentation, also increases the cellular surface area for oxygen uptake.

2.3.3 *R. oryzae* immobilisation process

R. oryzae forms an immobilised biofilm when grown under high shear conditions. It was shown that *R. oryzae* only produces high titre fumarate under nitrogen-limited conditions (Naude & Nicol, 2018a), making organism growth and fumarate production in the same reaction medium very ineffective. A strategy was devised to switch to a new nitrogen-free reaction medium mid-experiment by initially starting with excess glucose and the nitrogen available, then double washing the immobilised biomass and filling the reactor with a nitrogen-free medium (Naude & Nicol, 2018a). Ethanol remains an unwanted byproduct during this acid production reaction phase, regardless of excess O_2 availability. All experiments were conducted in a novel immobilised bioreactor system that was designed and utilised by the Bioreaction Engineering research group at the University of Pretoria and previously used by Naude & Nicol (2017), Naude & Nicol (2018a), and Naude & Nicol (2018b) and Swart *et al* (2020). This bioreactor system allows tight control over the biomass film thickness produced by manipulating the glucose concentration of the growth medium, avoiding the necessity for complicated mobilised biomass pellet production. The biomass immobilisation capacity of this novel system accommodates simple, rapid and sterile transition between different reaction media, specifically the growth, rinsing and production media. Images of *R. oryzae* immobilised biofilm in a bioreactor setup are presented in Figure 4.

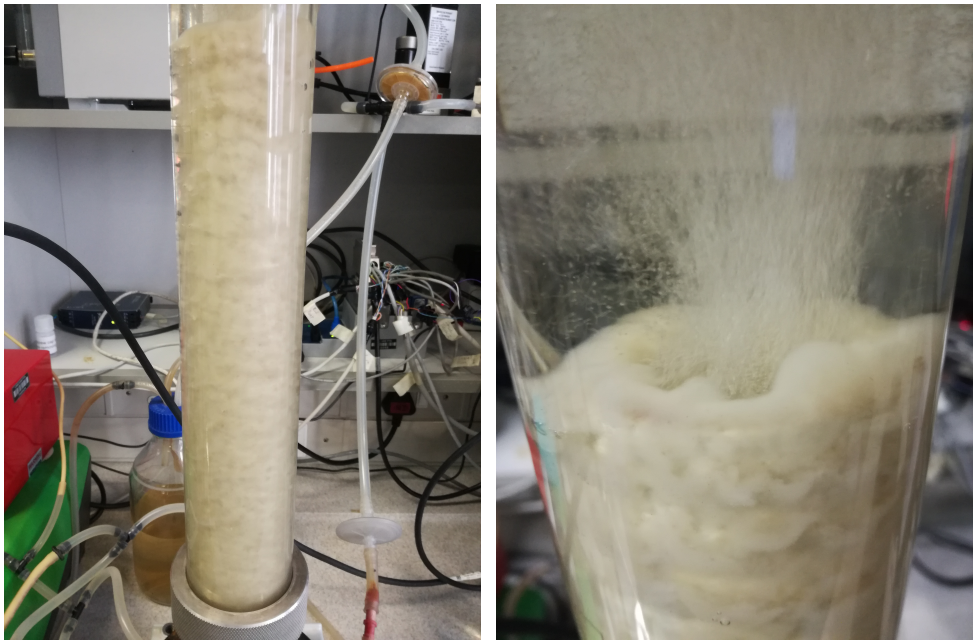

(a) **(b)**

Figure 4: Images of *Rhizopus oryzae* immobilised biofilm in a bioreactor setup.

2.4 Glucose overflow

2.4.1 Crabtree effect in *Saccharomyces cerevisiae*

Bakers' yeast (*Saccharomyces cerevisiae*) is known to produce ethanol under full aerobic conditions due to an oversupply of glucose in the reaction medium. During cellular respiration, glucose undergoing glycolysis produces pyruvate. The preferred method of obtaining energy from pyruvate is through aerobic respiration, where all pyruvate is oxidised to CO_2 in the TCA cycle to produce cellular energy (ATP), which consumes O_2 in the process. The cellular O_2 uptake rate during aerobic respiration is limited to a certain maximum enzymatic rate, resulting in a maximum rate at which pyruvate may be broken down by the TCA cycle. As cellular glucose intake is normally not naturally inhibited at low glucose concentrations, all excess pyruvate must then be channelled to an alternative carbon sink (overflow), which is ethanol in the case of *S. cerevisiae*. This glucose metabolic overflow phenomenon is called the Crabtree effect (Deken, 1966). Organisms that are Crabtree-positive have the ability to consume glucose at a faster rate than Crabtree-negative organisms, leading to a higher metabolic energy production rate as energy produced via the TCA cycle may now be supplemented with additional energy produced via a fermentative pathway such as ethanol production. *R. oryzae*, like *S. cerevisiae*, exhibits a glucose overflow mechanism and has been proved to be Crabtree-positive (Swart *et al*, 2020). Swart et al. have shown clearly that full aerobic condition ethanol

production may be eliminated by throttling the organism's glucose supply rate to a value below the overflow point (Swart *et al*, 2020). The excess glucose consumed, not fluxing through the TCA cycle or towards biomass production, instead forms ethanol (fermentation) and not solely CO_2 (respiration). The presence of ethanol inhibits the growth of *R. oryzae* at high concentrations and may be used as a carbon source at low concentrations (Dantigny *et al*, 2005). The substrate is wasted on producing low-value ethanol, rather than high-value fumarate, resulting in less profit. An additional downstream separation process is necessary to separate multiple products, increasing the process capital and running costs. It is therefore desirable to avoid ethanol production altogether by eliminating the overflow effect. This is achievable by operating in a substrate-limited regime where the glucose available is sufficient only for cell respiration (Swart *et al*, 2020).

2.4.2 Respiration quotient control in microorganisms

Numerous studies done on *S. cerevisiae* have shown that it is possible to alter yeast cell growth and ethanol production by controlling the organism respiration quotient (RQ) via glucose feed addition rate manipulation (XC Zhang *et al*, 1994; Woehrer & Roehr, 1981). RQ control may also be implemented for arachidonic acid production by *Mortierella alpina* (Li *et al*, 2018). A similar fed-batch strategy of eliminating the overflow metabolism of Crabtree-positive organisms was attempted by Habegger et al. (Habegger, Crespo & Dabros, 2018), by controlling the organism-specific growth rates of *S. cerevisiae* and *Escherichia coli*, respectively. Here biomass concentration was measured online via dielectric spectroscopy and turbidity measurements, and glucose was fed according to a feedforward-feedback control scheme. This approach and controller algorithm was later refined on *Kluyveromyces marxianus* (Brignoli *et al*, 2020). A root mean square specific growth rate control error of $23 \pm 6\%$ is reported by Brignoli et al. using an optimised, novel proportional-integral (PI) feedforward-feedback controller with a first-order Savitzky–Golay noise filter algorithm (Brignoli *et al*, 2020). Butkus et al. also propose a strategy based on fuzzy logic for specific growth rate adaptive control of *E. coli* (Butkus, Repšyte & Galvanauskas, 2020).

As *Rhizopus oryzae* is also regarded as a Crabtree-positive organism (Swart *et al*, 2020), it should be possible to utilise this same mechanism to eliminate ethanol production entirely, causing the organism to produce only biomass and CO_2. This could prove to be an efficient biomass growth strategy that would significantly improve biomass yield and would condition the cells to produce no alcohol dehydrogenase (ADH), improving transition to the acid production phase. By controlling the organism RQ at a certain value via glucose feed addition manipulation, a high final yield of biomass could be obtained with no ethanol, and thus no ADH, content.

The desired effect of spending glucose on only the organism anabolism and respiration could be achieved only if a suitable RQ-value range is selected for exploration. If a theoretical batch fermentation is considered as a starting point for RQ-range determination, we would expect the resulting RQ to be higher than what we desire because additional CO_2 would be present, originating from significant ethanol formation and some CO_2 being consumed during fumarate production. The theoretical desired RQ may be described as:

$$RQ^{desired} = \frac{r_C^{X\ +\ resp}}{r_O^{tot}} \tag{4}$$

where $RQ^{desired}$ is the desired RQ at which only biomass production and respiration takes place in $\mathrm{mol\,mol^{-1}}$, r_O^{tot} is the total O_2 consumption rate in $\mathrm{mol\,l^{-1}\,h^{-1}}$, $r_C^{resp\ +\ X}$ is the rate at which CO_2, originating from only biomass production and respiration, is produced in $\mathrm{mol\,l^{-1}\,h^{-1}}$, calculated by:

$$r_C^{X\ +\ resp} = r_C^{tot} + r_C^{FA} - r_C^{E} \tag{5}$$

where r_C^{tot} is the total CO_2 production rate in $\mathrm{mol\,l^{-1}\,h^{-1}}$, r_C^{FA} is the CO_2 consumption rate during fumarate production in $\mathrm{mol\,l^{-1}\,h^{-1}}$ and r_C^{E} is the CO_2 production rate during ethanol production in $\mathrm{mol\,l^{-1}\,h^{-1}}$. The liquid metabolite-dependent CO_2 rates, r_C^{FA} and r_C^{E} may be determined as:

$$r_C^{FA} = 0.25 r_{FA} \tag{6}$$

and

$$r_C^{E} = 0.5 r_E \tag{7}$$

where r_{FA} is the fumarate production rate in $\mathrm{cmol\,l^{-1}\,h^{-1}}$ and r_E is the ethanol production rate in $\mathrm{cmol\,l^{-1}\,h^{-1}}$. A suitable variance may then be selected around $RQ^{desired}$ for experimental exploration.

A theoretical estimated ideal RQ may also be calculated by replacing Equation 5 with:

$$r_C^{X\ +\ resp,estimate} = 0.1 r_X + r_O \tag{8}$$

where $r_C^{X\ +\ resp,estimate}$ is an estimated rate at which CO_2, originating from only biomass production and respiration, is produced in $\mathrm{mol\,l^{-1}\,h^{-1}}$.

3 Experimental

3.1 Microorganism and culture conditions

R. oryzae (ATCC 20344) obtained from the Spanish collection of cultures (Colección Española de Cultivos Tipo, Valencia, Spain) was prepared as described previously by Naude and Nicol (Naude & Nicol, 2017). Cultures were grown on potato dextrose agar (PDA) plates for 96 h at 35 °C to induce spore production. Spores were separated from the plates by washing with distilled water and hydrated at 25 °C for 12 h without agitation before being injected. Spore concentrates were checked for contamination by inoculating a growth medium similar to the reaction medium at 35 °C and testing for any unknown or contamination-indicative metabolites via high performance liquid chromatography (HPLC) analysis.

The number of passages, and therefore unintended mutations, was minimised by growing a large number of spores on PDA and preserving them by means of storage at -40 °C in a 50% glycerol solution. Inocula are prepared from these sub-zero cultures by making a large number of culture plates. Culture plates were incubated at 35 °C for 96 h until sufficient sporulation had occurred and then stored at 4 °C for up to two weeks, before being discarded.

The inoculum consisted of a 10 ml solution containing 8×10^6 spores ml^{-1}, prepared by adding distilled water to one of the cultured plates and carefully mixing to suspend the spores, but not disturb the agar. This suspension was sucked up into a 10 ml syringe and left overnight to hydrate the spores. A 21 gauge needle was then attached in a sterile environment and heated under a naked flame until glowing before being injected into the reactor vessel via a silicon septum. Once the needle had cooled, the contents were injected into the reactor and the tubing between the injection point and the reactor was clamped off to prevent contamination. Any variation in inoculum size or spore concentration was mitigated by defining an experimental starting point immediately after 2 g of glucose had been consumed batchwise.

3.2 Medium

The composition of the experimental growth medium is presented in Table 1.

Table 1: Growth medium composition.

Compound	**Batch** ($g\,l^{-1}$)	**Fed-batch init.** ($g\,l^{-1}$)	**Fed-batch washed** ($g\,l^{-1}$)
Glucose	6	2	0
Urea	2	2	2
KH_2PO_4	0.6	0.6	0.6
$MgSO_4 \cdot 7H_2O$	0.25	0.25	0.25
$ZnSO_4 \cdot 7H_2O$	0.088	0.088	0.088
$FeSO_4 \cdot 7H_2O$	0.0005	0.0005	0.0005

The fed-batch glucose feed concentration was $100\,g\,l^{-1}$. Medium components were sourced from Merck (South Africa). All medium solutions were prepared with distilled water and sterilised at 121 °C for 1 h in an autoclave. Glucose, urea, sulphates and phosphates were sterilised in separate containers and combined once they had cooled to room temperature to prevent irreversible mineral precipitation reactions from occurring while at high temperatures.

3.3 Fermentation

The in-house designed and locally produced novel reactor used was a modified version of that used by Naude and Nicol (Naude & Nicol, 2017). The setup process flow diagram is presented in Figure 5, with the numbers relating to equipment pieces as follows: 1: Nitrogen (urea), 2: Phosphates, 3: Sulphates, 4: Acid neutraliser (HCl), 5: Base neutraliser (NaOH), 6: Liquid/gas separator, 7: CO_2, 8: Air, 9: Substrate (glucose), 10: Gas analyser, 11: pH and temperature probe, 12: Samples, 13: Gas analyser outlet, 14: Process gas outlet, 15: Sampling pump, 16: Dosing pump, 17: Liquid recycle pump, 18: Gas recycle pump, 19: Gas flow controller (CO_2), 20: Gas flow controller (Air), 21: Syringe, 22: Septum, 23: Inoculation line, 24: Level control line, 25: Reactor cap, 26: Gas space, 27: Liquid space, 28: Growth scaffold, 29: Gas sparger, 30: Outer port, 31: Middle port, 32: Inner port, 33: Reactor base, 34: Heating plate.

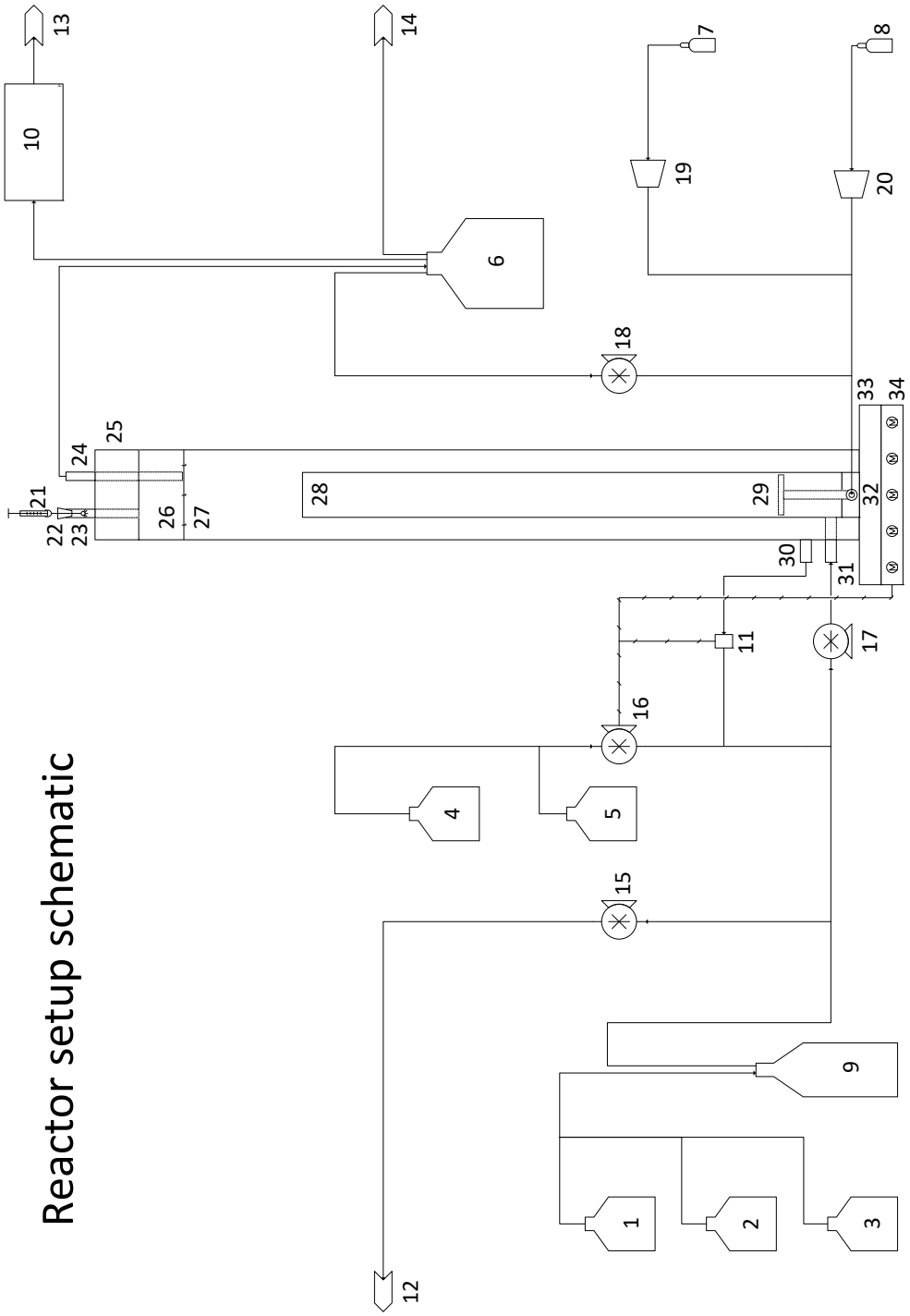

Figure 5: Experimental setup process flow diagram. 1: Nitrogen (urea), 2: Phosphates, 3: Sulphates, 4: Acid neutraliser (HCl), 5: Base neutraliser (NaOH), 6: Liquid/gas separator, 7: CO_2, 8: Air, 9: Substrate (glucose), 10: Gas analyser, 11: pH and temperature probe, 12: Samples, 13: Gas analyser outlet, 14: Process gas outlet, 15: Sampling pump, 16: Dosing pump, 17: Liquid recycle pump, 18: Gas recycle pump, 19: Gas flow controller (CO_2), 20: Gas flow controller (Air), 21: Syringe, 22: Septum, 23: Inoculation line, 24: Level control line, 25: Reactor cap, 26: Gas space, 27: Liquid space, 28: Growth scaffold, 29: Gas sparger, 30: Outer port, 31: Middle port, 32: Inner port, 33: Reactor base, 34: Heating plate.

The reaction liquid volume was 1 l with a gas phase volume of 0.3 l. The polypropylene growth scaffold tube had a length of 386.5 mm and outer and inner diameters of 40 mm and 32 mm respectively. The scaffold was fixed to the base to provide a boundary between the middle and outer base ports. The inner and middle base ports are connected via the inner, hollow side of the growth scaffold. A 79% N_2/21% O_2 Afrox instrument-grade synthetic air mixture and Afrox instrument-grade CO_2 were sparged through the reactor via Brooks Delta II smart mass flow controllers (Hatfield PA, USA) at flow rates of 90 $\mathrm{ml\,min^{-1}}$ and 10 $\mathrm{ml\,min^{-1}}$, respectively. Atmospheric pressure was 86 kPa. The liquid temperature, measured with the pH probe, was controlled and kept constant at 35 °C, with the heating plate on which the reactor was positioned as the actuator.

The reactor itself consists of a separate base, cap and body. The cap is made of aluminium, the body of borosilicate glass and the base partly of 304 stainless steel (upper part) and partly of mild steel (lower part).

Both the cap and base have numerous ports permitting the injection and ejection of various materials. The cap ports are utilised for inoculum injection, feed or base addition and level control. The base ports give access to three separate sub-volumes of the reactor, namely an inner, middle and outer section, as illustrated. The inner base port is used solely for gas injection. The middle and outer ports are connected externally via a peristaltic liquid recycle pump (Watson-Marlow 323U from Johannesburg, South Africa) operating at a constant rate of 833.3 $\mathrm{ml\,min^{-1}}$, alternating direction every 2 min, to facilitate the approximation of a perfectly mixed tank reactor and internally via the liquid sub-volume above the growth scaffold. This prevents any growth from occurring inside the connection tubes between process components via high shear forces. The reactor outlet gas is recycled at 521.7 $\mathrm{ml\,min^{-1}}$ (Watson-Marlow 520S) to increase the gas-sparging flow rate, improving gas diffusion throughout the reactor volume.

Three respective pumps are used for feeding, dosing and sampling (all Watson-Marlow 120U). The sampling frequency is chosen so that approximately eight to twelve samples are taken per stage for every experiment. The initial medium pH at inoculation was measured at 6.5 with a CPS171D glass pH probe from Endress & Hauser (Gerlingen, Germany) housed within an aluminium probe holder situated in the recycle line. All pH measurements were taken and appropriate dosing implemented with an Endress & Hauser Liquiline CM442 transmitter. As organic acids were produced during batch fermentations, the pH was controlled, by dosing 10 M NaOH, so as not to drop below 5.0. As little to no acids were produced during fed-batch fermentations, the pH remained relatively constant, but was not controlled, at the initial value of 6.5. The feed pump is used to feed a concentrated glucose solution to the reaction medium according to a number of feed addition strategies.

The reactor effluent gas flow is utilised to control the liquid level in the reactor. As the liquid level reaches the height of the level control tube, gas pressure pushes surplus liquid through the tube and into the liquid-gas separator (liquid trap). The effluent gas then passes through a Magellan Instruments Tandem Gas Analyser model 0588-TGA (Borehamwood, UK), which determines the gas O_2 and CO_2 content. The respective CO_2 production and O_2 consumption rates are then calculated according to:

$$r_C = \frac{K}{V_l}\{[Q^f_{CO_2} - Q^f_{tot}(y^{cal}_{CO_2})] - V_g \frac{d}{dt}(y^{cal}_{CO_2})\} \tag{9}$$

and

$$r_O = \frac{K}{V_l}\{[y^{air}_{O_2} Q^f_{air} - Q^f_{tot}(y^{cal}_{O_2})] - V_g \frac{d}{dt}(y^{cal}_{O_2})\} \tag{10}$$

respectively, where r_C and r_O are the respective CO_2 production and O_2 consumption rates in $\mathrm{mol\,l^{-1}\,h^{-1}}$; K is the conversion factor, equal to 2.373×10^{-3}, $y^{air}_{O_2}$ $\mathrm{mol\,min\,ml^{-1}\,h^{-1}}$; V_l is the reactor liquid phase volume in l; $y^{air}_{O_2}$ is the mole fraction O_2 in the air feed stream; $Q^f_{CO_2}$ and Q^f_{air} are the respective inlet CO_2 and air gas feed flow rates in $\mathrm{ml\,min^{-1}}$; Q^f_{tot} is the total gas feed flow rate in $\mathrm{ml\,min^{-1}}$; $y^{cal}_{CO_2}$ and $y^{cal}_{O_2}$ are the respective CO_2 and O_2 calibrated effluent gas mole fractions; V_g is the reactor gas phase volume in l and t is time in h. The respective CO_2 and O_2 calibrated effluent gas mole fractions may be calculated as:

$$y^{cal}_{CO_2} = y_{CO_2} - y^{baseline}_{CO_2} + \frac{Q^f_{CO_2}}{Q^f_{tot}} \tag{11}$$

and

$$y^{cal}_{O_2} = y_{O_2} - y^{baseline}_{O_2} + y^{air}_{O_2}\frac{Q^f_{air}}{Q^f_{tot}} \tag{12}$$

respectively, where y_{CO_2} and y_{O_2} are the respective measured reactor effluent gas CO_2 and O_2 mole fractions and $y^{baseline}_{CO_2}$ and $y^{baseline}_{O_2}$ are the respective measured CO_2 and O_2 reactor effluent gas mole fractions at steady state before inoculation. The total reactor effluent gas flow rate is assumed to be approximately equal to the total gas inlet flow rate and is calculated by adding the inlet CO_2 and air flow rates together:

$$Q^f_{tot} = Q^f_{CO_2} + Q^f_{air} \tag{13}$$

A pH and temperature control system was purchased as a unit operation due to the need for detachable, autoclavable pH and temperature probes. A single probe is used to take both a temperature and a pH measurement. An internal control system was utilised for pH control and the dosing pump as actuator. A separate PID controller was designed for temperature control and programmed using the LabVIEW user interface.

All connector-tubing was Watson-Marlow Pumpsil silicon tubing, with the exception

of pump rotor interface, HCL and NaOH tubing, which was Watson-Marlow Marprene tubing.

Certain operational variables are controlled automatically - via computer user input, and others are controlled manually - via direct instrument panel user input. The control strategy implemented allows for automatic variable inlet gas flow and inlet gas composition via two separate gas flow controllers. The inlet nutrient mix (media) flow rate is controlled automatically via two pumps; nutrient addition could, however, be modified by enabling multiple separate media element (glucose, urea, etc.) inlet flow rates via the incorporation of additional pumps which could be controlled separately. The liquid recycle (mixing) flow rate and direction is controlled automatically via a single pump. The gas recycle flow rate (sparging rate) is controlled manually via a single pump.

A National Instruments data acquisition housing (DAQ), relay, power supply and input and output modules were used for reactor control and data acquisition.

Experiments were run continuously and liquid metabolite HPLC concentration data were converted to rate data by performing a mass balance over the liquid phase of a continuously stirred tank reactor, described by:

$$r_i = \frac{dc_i}{dt} - c_i^f D + c_i D \tag{14}$$

where r_i are the respective liquid metabolite rates in $\mathrm{cmol\,l^{-1}\,h^{-1}}$; c_i are the respective reactor outlet liquid metabolite concentrations in $\mathrm{cmol\,l^{-1}}$; t is time in h; c_i^f are the respective reactor feed liquid metabolite concentrations in $\mathrm{cmol\,l^{-1}}$; and D is the dilution rate in $\mathrm{h^{-1}}$, calculated as:

$$D = \frac{Q_{liq}^f}{V_l} \tag{15}$$

where Q_{liq}^f is the reactor total liquid feed rate in $\mathrm{l\,h^{-1}}$.

All liquids were autoclaved prior to being fed into the reactor system. The entire reactor system, along with the pH probe, was also autoclaved prior to startup. Any entry and exit points open to the atmosphere were fitted with air filters to prevent contamination. The feed was connected to the reactor system via metal connectors fitted with ball valves. Prior to connection, the valves were shut. After both the feed and reactor system had been autoclaved separately, they were connected via the metal fittings. This combined connection was then left in a silicon oil bath at 140 °C for 20 min. Inoculum preparation took place in a laminar flow hood. All non-sterile materials used were sterilised with a 70% ethanol solution before use.

3.4 Growth strategies

A medium containing 6 g glucose, 2 g urea and minerals (see Table 1) was batch fermented with *R. oryzae* until full glucose depletion. All attempts at growth strategy improvement were fed-batch experiments. An initial amount of biomass, referred to as starter biomass, was grown batchwise with 2 g of glucose in the medium before the immobilised cells (as part of a naturally produced fungal mat biofilm on a coarse polypropylene tube) were washed twice with a mineral solution, and the glucose feed strategy was initiated for each respective fed-batch run, feeding 4 g of glucose over time. The same total amount of 6 g glucose was consumed in the batch experiment and all fed-batch experiments. The yield results of biomass on glucose were compared with respect to the biomass produced from the fed 4 g glucose and the corresponding consumed 4 g glucose in the respective fed-batch and batch experiments.

The cellular ethanol production rate was controlled by altering the glucose addition rate. Effluent gas composition was measured online, enabling instantaneous feed rate manipulation, controlling the RQ. A proportional-integral (PI) controller was implemented for this purpose, keeping the organism's RQ at 1.3 and 1.1 for experiments RQ1.3 and RQ1.1, respectively. Glucose was fed at a constant rate of 0.075 $\mathrm{g\,h^{-1}}$ for experiment CGF.

The glucose feed rate controller output was determined by:

$$r_S^f = K_P * (e + \frac{1}{T_I} I_{term}) \tag{16}$$

where r_S^f is the glucose feed rate, K_P is the proportional gain constant, e is the error value (the difference between the controlled variable set point and the measured value, T_I is the integral time constant), and I_{term} is the current accumulative integral term. The current accumulative integral term was calculated by:

$$I_{term} = I_{term}^{t-1} + e \tag{17}$$

where I_{term}^{t-1} is the accumulative integral term calculated from the start of controlled feed initiation up until the previous measurement time (previous second). The error was calculated as:

$$e = SP - RQ_{meas} \tag{18}$$

where SP is the controlled variable set point and RQ_{meas} is the controlled variable (RQ) measured value passed through a 10 min simple moving average filter.

3.5 Analytical methods

The concentrations of the liquid metabolites, namely glucose, ethanol, fumarate, malate, pyruvate and glycerol were measured via HPLC with an Aminex HPX-87H ion exchange column (Bio-Rad Laboratories, USA) equipped with a refractive index (RI) detector (55 °C) and a 300 mm × 7.8 mm Aminex HPX-87H ion-exchange column (Bio-Rad Laboratories, USA). Standard curves for these compounds were generated by plotting the area under the resulting peaks against known concentration values before fitting a straight line through the origin and at least two other known points. Standard concentration and coefficient of determination (R^2) values for each compound are provided in Table 2.

Table 2: HPLC standard concentration and coefficient of determination (R^2) values for glucose, ethanol, fumarate, malate, pyruvate and glycerol.

Compound	Conc. ($g\,l^{-1}$)	R^2	Compound	Conc. ($g\,l^{-1}$)	R^2
Glucose	0.1001	1.00000	Malate	0.1099	1.00000
	1.001			1.099	
	10.01			10.99	
Glycerol	0.1009	0.99988	Pyruvate	0.1021	0.99997
	1.009			1.021	
	10.09			10.21	
Fumarate	0.1039	0.99587	Ethanol	0.9898	1.00000
	1.039			9.898	

Both mobile phase (phase A: 1.95 $g\,l^{-1}$ H_2SO_4, phase C: 0.53 $g\,l^{-1}$) flow rates were 0.6 $ml\,min^{-1}$ with a column temperature of 60 °C, as previously described by Naude and Nicol (Naude & Nicol, 2017). The reactor mixed-phase effluent was separated into gas and liquid phases. The liquid phase was discarded and the gas phase composition analysed online. A Tandem Gas Analyser (Magellan Biotech, UK) was used to measure effluent gas CO_2 and O_2 concentrations, also as previously described by Naude and Nicol (Naude & Nicol, 2017). Reactor steady-state gas composition was determined before culture inoculation and used as a baseline for zero metabolic gas activity. Immobilised biomass on the polypropylene growth scaffold was removed, washed, dried and weighed, again as previously described by Naude and Nicol (Naude & Nicol, 2017).

4 Results and Discussion

4.1 Limit-switch control

4.1.1 Respiration quotient range analysis

A comprehensive kinetic model for *R. oryzae* may be obtained from two previous publication by Naude and Nicol (Naude & Nicol, 2017) (Naude & Nicol, 2018a).

It is often attempted to manipulate Crabtree-positive organism overflow metabolisms by controlling the respective organism-specific growth rate (Habegger *et al*, 2018; Brignoli *et al*, 2020; Butkus *et al*, 2020). One major challenge of this approach is accurately estimating the current specific growth rate based on online biomass concentration measurements (Habegger *et al*, 2018). Biofilm formation, air-liquid bubble dynamics and changes in medium conductivity caused by the addition of base and feed may produce large measurement inaccuracies, whereas online RQ measurements are independent of these factors and provide, overall, far less noisy data. As specific growth rate controller algorithms often contain exponential terms, a sudden change in the measured error value may result in an exaggerated controller output, possibly causing system instability. The linear nature of RQ controller algorithms results in a less-exaggerated controller response, thereby aiding system stability.

The RQ provides a direct indication of active metabolic fluxes. When only respiration is considered the RQ will have a value of unity since a mole of CO_2 is formed for each mole of O_2 consumed. Biomass growth is typically associated with the formation of anabolic CO_2 and hence the RQ is expected to be slightly higher than unity when respiration energy is the sole driver for growth. Ethanol formation is caused by high glucose concentrations in the broth, which enhances glucose uptake beyond the respiratory capacity of the cell. Since ethanol formation is associated with the coformation of CO_2, a higher RQ is likely to result if fumarate formation is small or negligible (fumarate formation is associated with the uptake of CO_2, which would reduce the RQ). Controlling the RQ via feed manipulation thus implies that the flux distribution within the cell is controlled.

According to the metabolic map of *R. oryzae*, if only respiration is considered, every mole of CO_2 produced requires one mole of O_2 to be consumed; resulting in a theoretical minimum organism RQ of 1.0 $\mathrm{mol\,mol^{-1}}$. Analysis of the batch liquid and gas metabolite rate profiles is presented in Figure 6, revealing that the ideal RQ-value where only biomass production and respiration occur lies approximately between 1.0 and 1.3 (Figure 6a). Figure 6 also shows the CO_2 rate contributions from ethanol formation (r_C^E), fumarate

formation ($-r_C^{FA}$), respiration ($r_C^{respiration}$), the total CO_2 production rate (r_C^{tot}) and the calculated resulting CO_2 production rate if only biomass formation and respiration are considered ($r_C^{X+respiration}$) (Figure 6b).

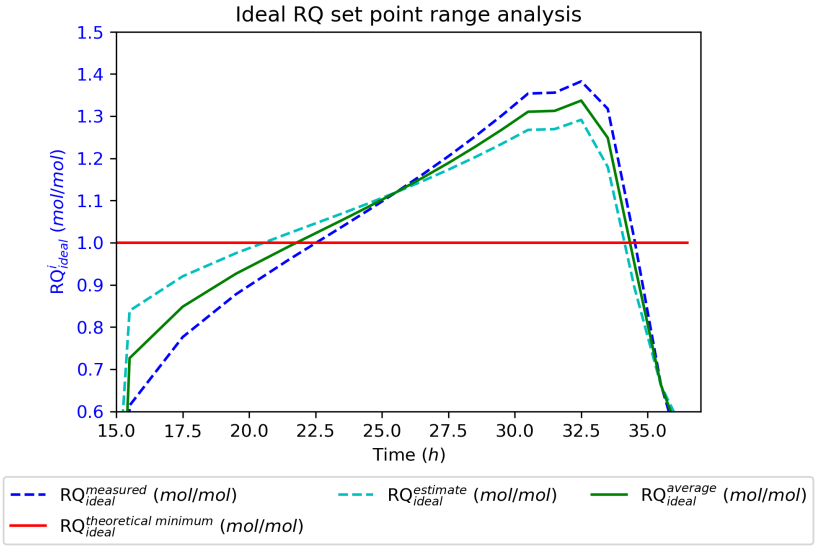

(a)

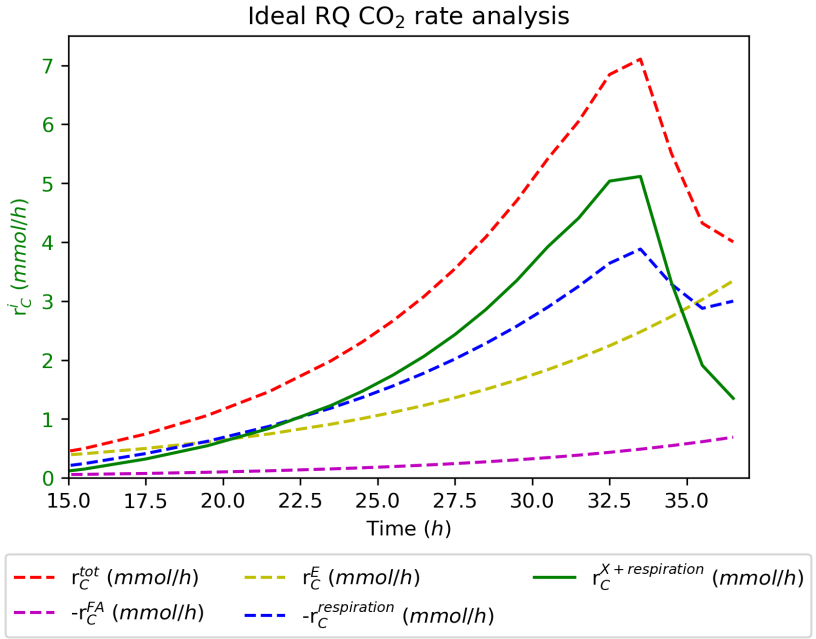

(b)

Figure 6: CO_2 rate analysis and calculation of the ideal RQ-value where only biomass production and respiration occur, lying approximately between 1.0 and 1.3.

Glucose addition was controlled by maintaining a constant RQ at 1.3 initially, with both the limit-switch control and PI-control strategies, and later at 1.1 with the PI-control strategy.

4.1.2 Minimum glucose addition rate

Similarly to how the ideal RQ-range was determined, the net glucose consumption rate (glucose used only for respiration and biomass formation) was determined by subtracting all undesired product streams from the overall glucose consumption rate of a batch fermentation, mathematically described as:

$$-r_S^{net} = -r_S^{tot} - (-r_S^{liq\ met} + r_C^E - r_C^{FA}) \tag{19}$$

where r_S^{net} is the net glucose consumption rate required for only respiration and biomass production, r_S^{tot} is the total glucose consumption rate, and $r_S^{liq\ met}$ is the glucose consumption rate required to produce all liquid phase metabolites except biomass. All terms are in cmol l^{-1} h^{-1}. The $r_S^{liq\ met}$ term may be described as:

$$-r_S^{liq\ met} = r_{MA} + r_{PA} + r_{SA} + r_{LA} + r_{FA} + r_G + r_E \tag{20}$$

Once the net required glucose consumption has been determined, it should be possible to manipulate the organism to behave in the desired manner by feeding glucose at this rate. The active metabolic regime that the organism functions in is a function of the biomass-based (and not volumetrically-based) glucose consumption rate. It is therefore necessary to feed glucose at a certain rate at a certain biomass concentration. No direct biomass concentration measurement was available and the O_2 consumption rate was used as a proxy measurement for biomass concentration. Excess O_2 was supplied to the reactor throughout all experiments and it was assumed that all cells consumed O_2 at the maximum possible metabolic rate. The glucose consumption rate profiles and fitted O_2 consumption rate specific to the net glucose consumption rate, including the exponential correlation:

$$r_S^{fitted\ feed\ rate} = (6.79e-03)exp\{(-3.63e+02)[r_O + (1.58e-04)]\} - (6.87e-03) \tag{21}$$

where $r_S^{fitted\ feed\ rate}$ is the correlated glucose feed rate, are presented in Figure 7a and Figure 7b, respectively.

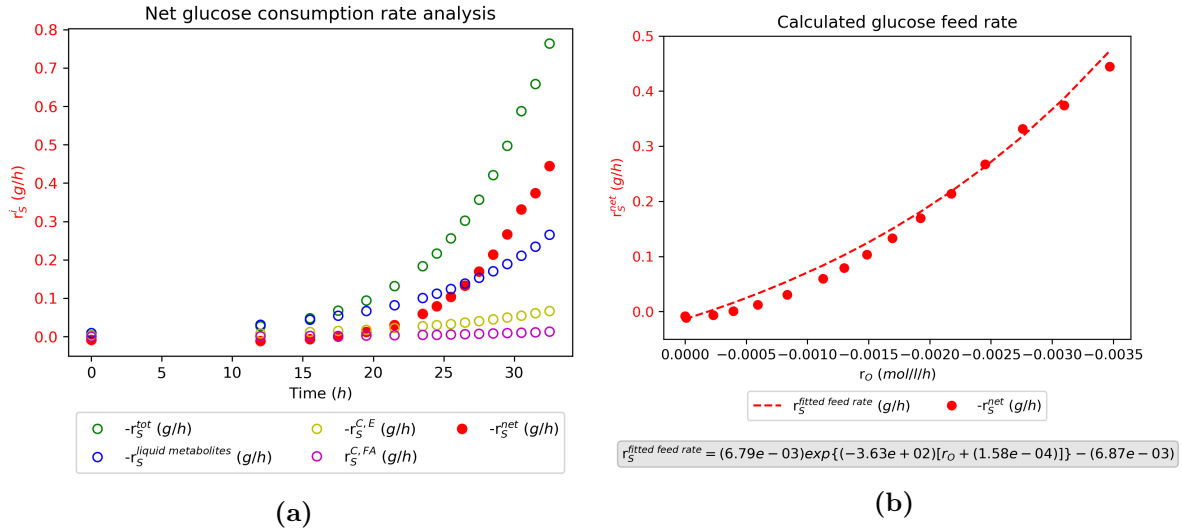

(a) **(b)**

Figure 7: Glucose consumption rate profile analysis (a) and fitted O_2 consumption rate specific net glucose consumption rate: $r_S^{fitted\ feed\ rate} = (6.79e-03)exp\{(-3.63e+02)[r_O+(1.58e-04)]\}-(6.87e-03)$.

4.1.3 Metabolic response

Glucose was fed according to the net glucose consumption correlation, after starter biomass had been grown batch-wise with 2 g of glucose and washed twice with mineral solution, until an additional 4 g glucose was dispensed. The correlated feeding algorithm was only implemented when the measured RQ was between 1.05 and 1.3 (normal-feed mode). A limit-switch mechanism was implemented, whereby the glucose feed rate was multiplied by 0.5 when the RQ was measured to be above 1.3 (low-feed mode), and multiplied by 1.5 when the RQ was measured to be below 1.05 (high-feed mode).

The resulting liquid phase metabolite concentration profiles are presented in Figure 8.

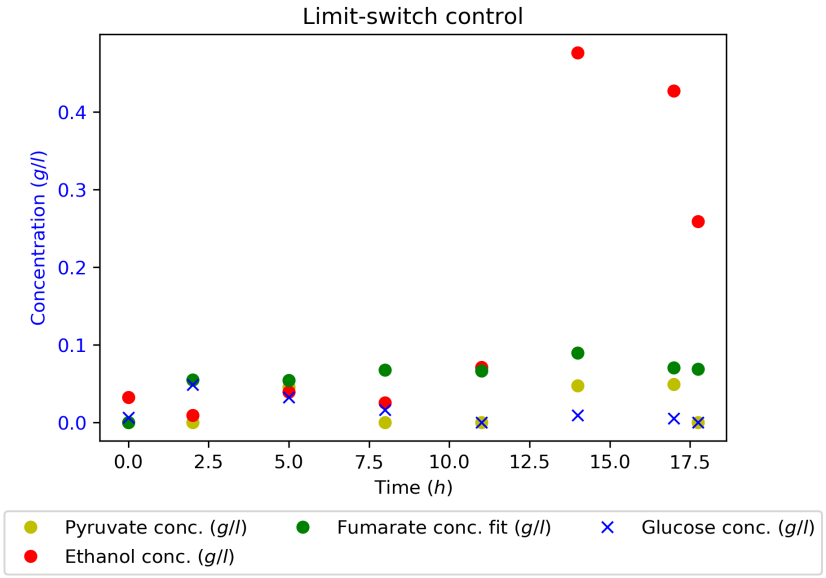

Figure 8: Liquid phase metabolite concentration profiles resulting from the glucose addition limit-switch control growth strategy.

A small amount of glucose buildup was observed, but only initially, while very low metabolite concentrations were detected from the start of the run until approximately 14 h. From 14 h onward, much higher ethanol concentrations are measured, while other metabolite concentrations remain relatively low. The observed ethanol formation after 14 h is probably due to a sudden shift in the RQ profile as a result of the high variance of the rapidly quasi-oscillating glucose feed rate.

The gas phase metabolite and feed rate profiles are presented in Figure 9.

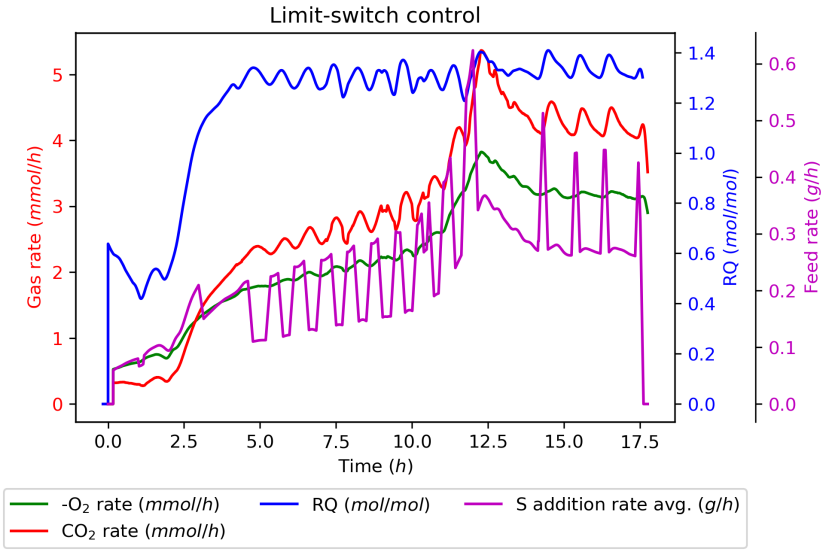

Figure 9: Feed rate and gas phase metabolite rate profiles resulting from the glucose addition limit-switch control growth strategy.

The system experiences an initial delay-phase until approximately 5 h, before the RQ-value reaches its operational range. Between 5 h and 12 h the system behaved as expected: the glucose feed rate, CO_2 production and O_2 consumption rates followed an exponentially increasing trend, while the RQ oscillated between approximately 1.25 and 1.35. As the RQ was often above the predefined limit of 1.3, the feed rate varied as the system switched between normal-feed mode and low-feed mode. The maximum feed rate was achieved at 12 h, followed by a partial collapse of the feed strategy. From 14 h until the end of the run, all profiles exhibit repeating profiles. In this last section RQ oscillates at higher values of between 1.3 and 1.4, which possibly explains the sudden initiation of ethanol production. A decrease in the CO_2 production and O_2 consumption rates was observed in this section, with both rate profiles exhibiting oscillatory behaviour. In the last section of the run glucose was fed, almost exclusively, on low-feed mode; however, only oscillatory behaviour, rather than an overall increase of the feed rate, was observed.

The accumulative O_2 consumed lies between that of the batch and RQ1.1 runs, but is slightly less, probably due to ethanol formation near the end of the run. A significant difference between the measured and predicted final biomass concentrations was observed. As in the CGF run, the exact explanation is unclear, but it is probably due to the oscillatory nature of the metabolite profiles, preventing operation at a steady RQ set-point. Missing carbon is likely to be present in the form of dissolved biomass, unaffected by the TOC sample pretreatment process and therefore is not accounted for.

The overall efficiency of the limit-switch control strategy is very limited compared with more sophisticated control strategies, such as PI-control. Even when operating as expected, the variance in the set-point value is exceedingly large, and when feed parameters are not adjusted dynamically, partial growth collapse may occur. In applications where conventional PID-type control strategies do not perform to satisfaction, these may be coupled with a net glucose (or other substrate) feed correlation for improved dynamic performance.

4.2 PI-control

4.2.1 Liquid phase

Using a PI-controller provides for much more stable process dynamics than using a limit-switch control strategy. The fed-batch runs, namely RQ1.3, RQ1.1 and CGF, were performed and analysed. Figure 10 displays the liquid metabolite concentrations for the batch and fed-batch runs.

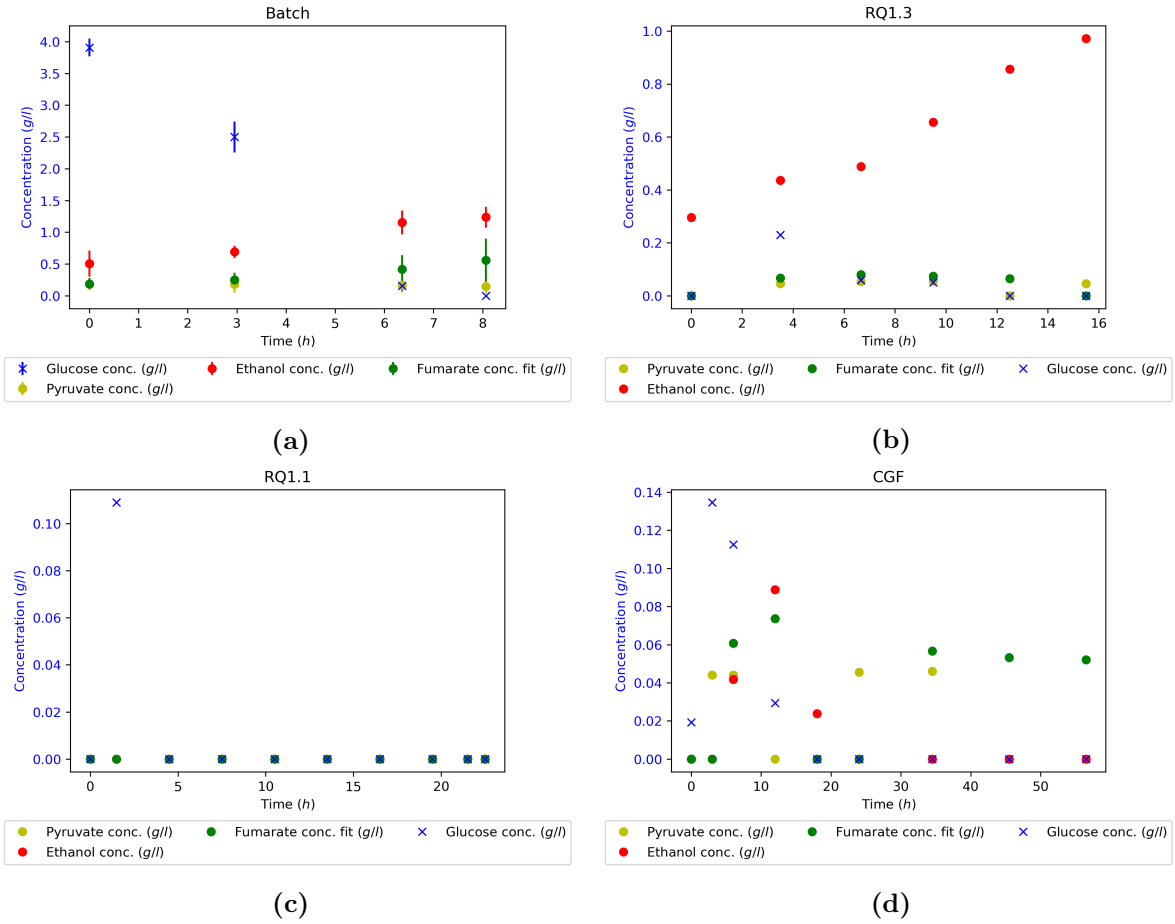

Figure 10: Liquid metabolite analyses of (a) batch, (b) RQ1.3, (c) RQ1.1, and (d) CGF. Ethanol production was observed for batch and RQ1.3, but not RQ1.1 and CGF. In addition to ethanol, significant amounts of pyruvate and fumarate were also produced during the batch experiment. Three batch experiments were performed; error bars represent the standard deviation.

The glucose consumption profile for the batch run follows a typical exponential trend. Significant amounts of ethanol and organic acids can be seen as a result of the high prevailing glucose concentrations during the batch run. Ethanol overflow is also clearly observed for the fed-batch run where the RQ was controlled at a value of 1.3. The fermentation time for the RQ1.3 run is double that of the batch run (see Table 3), indicating that the glucose flux was restricted in this run. Nevertheless, the glucose uptake restriction was not sufficient to negate ethanol formation. It can, however, be observed that the formation of fumaric acid is less than that of the batch run. For the RQ1.1 run it is clear that the overflow of ethanol and organic acids is completely eliminated, indicating that respiration was the only catabolic pathway. Note the longer fermentation time when comparing RQ1.1 with RQ1.3 (also see Table 3), indicating that the glucose uptake rates were lower for RQ1.1. The constant glucose feed run (CGF) took much longer than all the other runs due to the fact that the glucose addition flowrate was not increased as biomass accumulated. Apart from small amounts of ethanol formation

at the start of the run (at higher glucose concentrations), ethanol overflow was absent, as was expected from the low glucose uptake. Small amounts of organic acid excretion were observed in this run, unlike the RQ1.1 run where no organic acids could be detected.

Table 3: Experiment duration with corresponding biomass productivities and approximate average RQ-values.

	t (h)	P_X ($\mathrm{mg\,l^{-1}\,h^{-1}}$)	RQ_{avg} ($\mathrm{mol\,mol^{-1}}$)
batch	8.066	142.0	1.901
CGF	56.50	18.87	1.074
RQ1.3	15.50	86.74	1.281
RQ1.1	22.50	109.9	1.069

4.2.2 Gas phase

The composition of the reactor effluent gas stream was analysed for all experiments. Glucose, O_2 consumption and CO_2 production rates, as well as RQ, are presented in Figure 11.

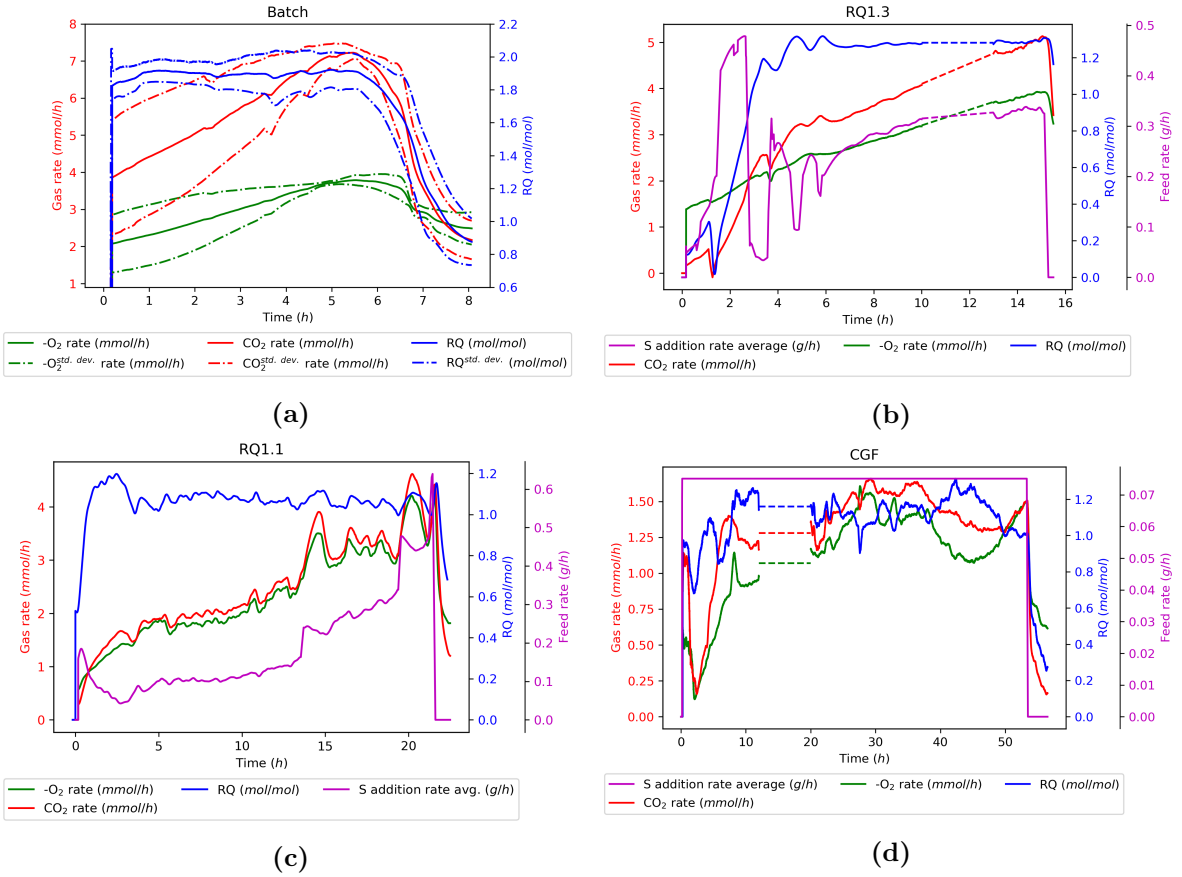

Figure 11: Gas analyses of (a) batch (3 runs) , (b) RQ1.3, (c) RQ1.1, and (d) CGF. A volumetric rate increase of gas and glucose over time, due to biomass growth, was observed in all runs except CGF. Dashed lines represent a graphical estimate of missing data due to gas analyser malfunction during the RQ1.3 and CGF runs. Three batch experiments were performed, with the dash-dotted lines representing the standard deviation.

For both the runs where the RQ was controlled the O_2 and CO_2 rates follow an increase with time as biomass accumulates. For the batch runs (performed in triplicate) the rate increase is also observed until a sudden drop occurs. This drop can be attributed to the depletion of the available glucose. For the CGF run the O_2 consumption and CO_2 production rates remain more constant, as expected.

The metabolite results from Figure 10 clearly indicate that the RQ1.1 run was sufficient in negating ethanol formation. The slightly larger amount of CO_2 produced compared with O_2 consumed can be attributed to the formation of anabolic CO_2 and it is safe to deduce that respiration was the only form of cellular ATP generation. For the RQ1.3 run ethanol formation contributed to ATP generation as can clearly be seen in Figure 10. In this run glucose was consumed faster than in the RQ1.1 run, but slower than in the batch run. The RQ control for the RQ1.3 run was slightly less efficient than that of the RQ1.1 run, mainly due to the glucose overshoot at the start of the fermentation. From

Figure 11 it is clear that tight RQ control is only achieved after 6 h and it is evident that ethanol formation continues beyond this time (Figure 10). The faster rate of glucose addition in RQ1.3 allows for a faster cellular glucose uptake and hence the respiration capacity of the cell is exceeded, causing ethanol overflow.

4.2.3 Biomass yield

Biomass yields are reported in Figure 12.

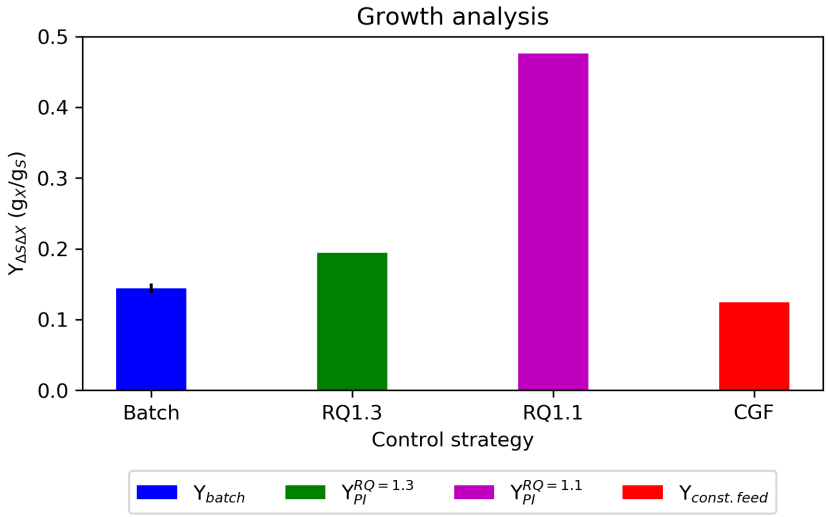

Figure 12: The biomass yield results for the four growth strategies. Calculated yields do not include starter biomass (first 2 g of glucose). The biomass yield of RQ1.1 is 3.3 times higher than that of the batch run. Three batch experiments were performed, with error bars representing the standard deviation.

Figure 12 clearly illustrates the advantage of controlling the RQ at the correct value. The biomass amount obtained with run RQ1.1 is 3.3 times higher than that of the batch run, while the RQ1.3 run results in a yield between that of the batch and RQ1.1 runs. More biomass is to be expected for the RQ1.1 run since all glucose is channelled to either biomass or respiratory CO_2. For the batch run the amount of metabolites (excluding CO_2) added up to a value of 2.09 g. This clearly indicates the wastage of glucose in the batch run, where ethanol, fumarate and pyruvate effectively remove the carbon that could have been used in the anabolism. It is interesting to note that the amount of waste metabolites decreases from 2.09 g for the batch run to 1.06 g for the RQ1.3 run. This makes sense given that the carbon uptake rate in the RQ1.3 run was less than that of the batch run. The low biomass yield for the CGF run is unexpected since the glucose uptake rates were even lower than those of the RQ1.1 run.

4.2.4 Mass balance checks and repeatability

Elemental mole balances were performed for C, H, O and N over the entire fermenter. In addition, all metabolite rate values were measured, except those of water and biomass production. The system may be fully mathematically described by solving for the rates vector in Equation 2, consisting of 13 equations, each of which represents a compound reaction rate from Equation 1. Equation 2 requires nine specified measured rate values (specifications) in addition to the four mole balances to solve the system. If a rate specification is not directly available, measured concentration data must be converted to rate data using Equation 14. As 10 specifications were already available (discounting biomass and water) along with the four elemental balances, only one overspecification was left. This additional specification was utilised to quantify gross measurement errors graphically through data reconciliation. No significant errors were observed.

Starter biomass values from the 2 g glucose batch fermentations were obtained from three separate experiments and are presented in Table 4.

Table 4: Starter biomass values from the 2 g glucose batch fermentations. Calculated relative standard deviation (RSD) to the average.

	Starter biomass (g)
Experiment 1	0.542
Experiment 2	0.549
Experiment 3	0.613
Average	0.568
RSD to average	0.056

Three separate batch fermentations were performed, for which liquid metabolite, off-gas, measured final biomass and mass balance predicted biomass analysis was performed. In Figure 10a the standard deviation is presented via error bars for liquid metabolites and in Figure 11a via dash-dotted line profiles for off-gas. The analysis of time, measured final and mass balance predicted biomass value is presented in Table 5.

Table 5: analysis of time, measured final ($m_X^{measured\ final}$) and mass balance predicted ($m_X^{predicted}$) biomass value. Calculated relative standard deviation (RSD) to the average.

	Time (h)	$m_X^{measured\ final}$ (g)	$m_X^{predicted}$ (g)
Experiment 1	8.5	1.107	1.007
Experiment 2	7.1	1.165	1.161
Experiment 3	8.6	1.164	1.315
Average	8.066	1.145	1.161
RSD to average	0.085	0.024	0.108

Two additional RQ1.3 experiments were performed to prove repeatability of the high biomass on glucose yield obtained previously. The total amount of glucose fed was not limited to only 4 g in these experiments as feed lines were submerged and diffusion into the reactor vessel occurred. The actual feed rate was back-calculated by setting the predicted final biomass concentration value equal to the measured final biomass concentration and solving for the mass balance over the system.

Very low amounts of ethanol were produced only initially in both runs and then consumed again in one of them. No liquid metabolite buildup was observed after the first 2 h from feed commencement. Some disturbances in the gas metabolite profiles were observed in the one experiment, while much better control was achieved in the other. An average RQ of approximately 1.1 was obtained in both repeats. The analysis of time, measured final biomass value, mass balance predicted fed glucose amount and biomass on glucose yield for the latter two experiments are presented in Table 6.

Table 6: Analysis of time, measured final biomass value ($m_X^{measured\ final}$), mass balance predicted fed glucose amount ($m_S^{predicted}$) and biomass on glucose yield ($Y_{SX}^{predicted}$) for the latter two RQ1.1 experiments. Calculated relative standard deviation (RSD) to the average.

	Time (h)	$m_X^{measured\ final}$ (g)	$m_S^{predicted}$ (g)	$Y_{SX}^{predicted}$ ($g\,g^{-1}$)
Experiment 2	14.5	3.359	5.560	0.502
Experiment 3	18.0	3.101	5.598	0.452
Average	16.25	3.230	5.579	0.477 [a]
RSD to average	0.108	0.040	0.003	0.042 [b]

[a] Average of all three repeats considered.

[b] RSD of all three repeats considered.

An overall mass balance over the entire timespan of each experiment was performed to calculate the theoretical amount of biomass formed using the assumed biomass elemental composition of $CH_{1.8}O_{0.5}N_{0.16}$. Given the overspecification, either the amount of O_2 consumed or the amount of CO_2 produced was emitted from the calculation. The results of the mass balances can be seen in Table 7.

Table 7: Overall mass balance results for the four growth strategies. Due to an overspecified system, either O_2 or CO_2 rates can be used as specification. Biomass relative error values based on O_2 and CO_2 mass balance specifications are denoted by $e_{O_2\ spec}^{relative}$ and $e_{CO_2\ spec}^{relative}$, respectively.

Exp	m_X^{meas} (g)	$m_X^{calc,O_2\ spec}$ (g)	$e_{O_2\ spec}^{relative}$	$m_X^{calc,CO_2\ spec}$ (g)	$e_{CO_2\ spec}^{relative}$
Batch	1.145	1.161	-0.014	1.246	-0.088
RQ1.3	1.344	1.313	0.023	1.682	-0.251
RQ1.1	2.473	2.367	0.043	2.594	-0.049
CGF	1.066	2.098	-0.967	2.116	-0.985

Both the O_2 and CO_2 specifications resulted in similar predictions, hinting at consistency in the measurements. The predictions of the batch, RQ1.1 and RQ1.3 runs were in good agreement with experimental data, with the O_2-based predictions resulting in a smaller error. For the CGF run both predictions were double those of the measured amounts. Performing a carbon mole balance over the entire reactor system indicates that a significant fraction of carbon is unaccounted for in the CGF run.

Figure 13 shows the accumulative O_2 consumption profiles for the respective runs and also includes the biomass measurements and predictions.

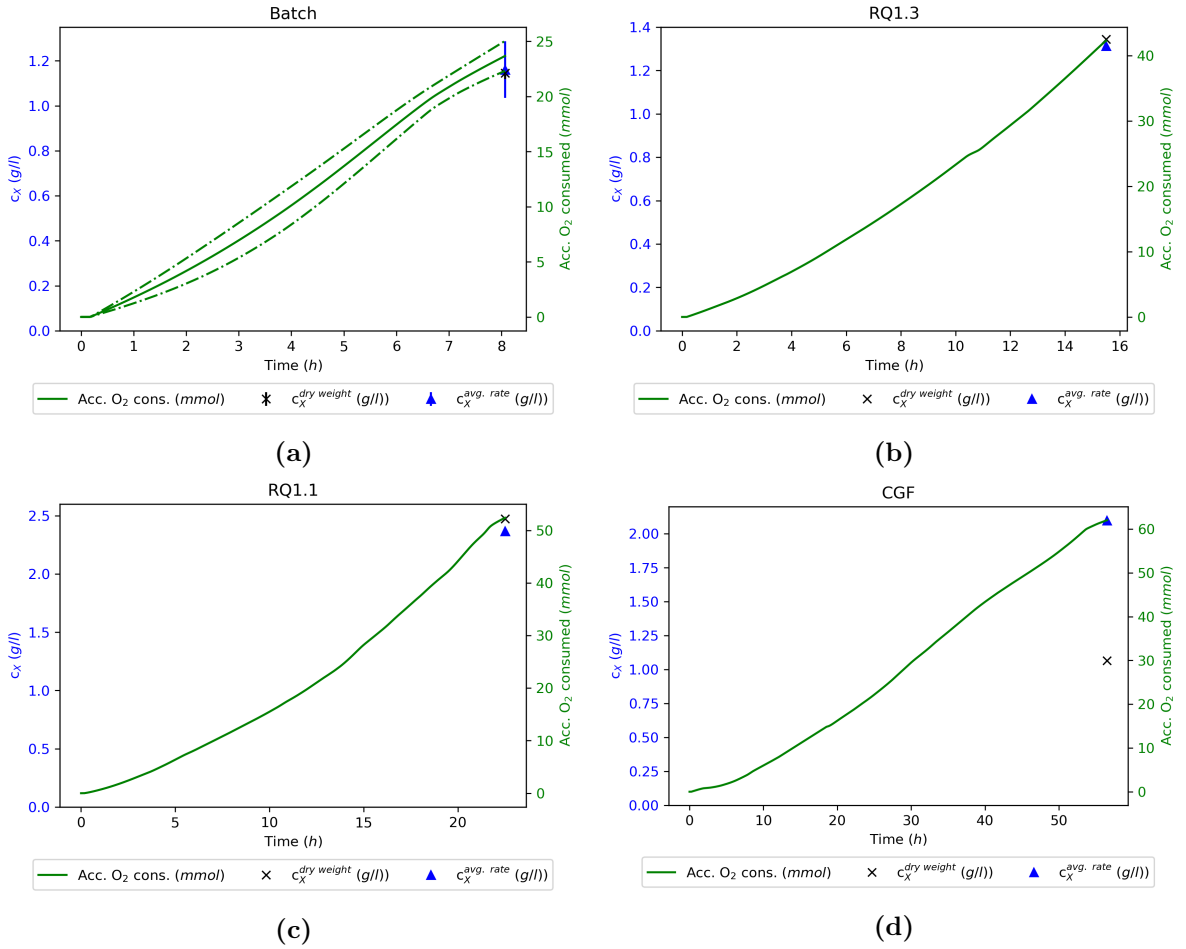

Figure 13: Overall mass balance results for the four growth strategies. Due to an overspecified system either the O_2 or CO_2 rates can be used as specification. Three batch experiments were performed; error bars and dash-dotted lines represent the standard deviation.

It can be clearly seen that the O_2 usage in the batch fermentation was the smallest. This relates directly to the fact that respiration contributed only partially to generating ATP within the cell. It is interesting to note that the RQ1.1 run, in which only respiration occurred, consumed double the amount of O_2 when compared with the batch run, while the RQ1.3 run resulted in an O_2 consumption between that of the batch and RQ1.1 runs. The CGF feed run consumed more O_2 than the RQ1.1 run and hence the biomass prediction in Table 7 and Figure 13 is slightly lower. The reason for the very low measured biomass is unclear. No additional metabolites were observed in HPLC sample analysis of the CGF run, and the total organic carbon (TOC) analysis of the final reactor broth yielded only 15 mg C l^{-1} in the form of non-immobilised cells or proteins, relating to only 0.05 g l^{-1} of biomass when using the assumed elemental composition for biomass.

5 Conclusion

The understanding of the Crabtree effect in eukaryotes in general and *R. oryzae* in particular was improved upon. Exploratory experiments were performed in which a fed-batch glucose addition strategy was developed to maintain *R. oryzae* cellular glucose intake rates below the maximum respiratory capacity. An acceptable RQ exploration range was determined via batch experiment data analysis. Preliminary exploratory results were obtained via a correlated glucose addition feed algorithm, using only the volumetric oxygen consumption rate as the independent variable. The PI-controller proved to be a clear improvement on the initial exploratory limit-switch controller. A slow feed addition strategy was employed, by which the feed rate was used to control the RQ via a PI-controller. Implementing a PI-controller to maintain a stable organism RQ, via glucose addition, provided much more sophisticated control over the organism's metabolic stability and resulted in *R. oryzae* being grown successfully without any ethanol or organic acids as byproducts.

A biomass on glucose yield more than three times higher than in batch fermentations was achieved by controlling the organism RQ at a value of 1.1, resulting in no byproduct formation apart from CO_2. The results presented contribute to the development of the immobilised or suspended biomass *R. oryzae* process. In addition, the growth strategy suggested will contribute to the improved efficiency of the fumarate and malate production process by *R. oryzae*.

References

Abe, A, Oda, Y, Asano, K and Sone, T (2007), "*Rhizopus delemar* is the proper name for *Rhizopus oryzae* fumaric-malic acid producers", *Mycologia*, 99 (5): 714–722, ISSN: 00275514, DOI: 10.3852/mycologia.99.5.714.

Bai, D, Jia, M, Zhao, X, Ban, R, Shen, F, Li, X and Xu, S (2003), "L(+)-lactic acid production by pellet-form *Rhizopus oryzae* R1021 in a stirred tank fermentor", *Chemical Engineering Science*, 58 (3-6): 785–791, ISSN: 00092509, DOI: 10.1016/S0009-2509(02)00608-5.

Bai, D, Zhao, X, Li, X and Xu, S (2004), "Strain improvement of *Rhizopus oryzae* for over-production of L(+)-lactic acid and metabolic flux analysis of mutants", *Biochemical Engineering Journal*, 18 (1): 41–48, ISSN: 1369703X, DOI: 10.1016/S1369-703X(03)00126-8.

Ban, K, Kaieda, M, Matsumoto, T, Kondo, A and Fukuda, H (2001), "Whole cell biocatalyst for biodiesel fuel production utilizing *Rhizopus oryzae* cells immobilized within biomass support particles", *Biochemical Engineering Journal*, 8 (1): 39–43, ISSN: 1369703X, DOI: 10.1016/S1369-703X(00)00133-9.

Baumann, A, Burns, D, Liu, B and Thoi, VS (2019), "Metal-organic framework functionalization and design strategies for advanced electrochemical energy storage devices", *Communications Chemistry*, 2 (1): 1–14, ISSN: 23993669, DOI: 10.1038/s42004-019-0184-6, URL: http://dx.doi.org/10.1038/s42004-019-0184-6.

Beauchemin, K and McGinn, S (2006), "Methane emissions from beef cattle: Effects of fumaric acid, essential oil, and canola oil", *Journal of Animal Science*, 84 (6): 1489–1496, ISSN: 00218812, DOI: 10.2527/2006.8461489x.

Bélafi-Bakó, K, Nemestóthy, N and Gubicza, L (2004), "A study on applications of membrane techniques in bioconversion of fumaric acid to L-malic acid", *Desalination*, 162 (1-3): 301–306, ISSN: 00119164, DOI: 10.1016/S0011-9164(04)00063-3.

Brignoli, Y, Freeland, B, Cunningham, D and Dabros, M (June 2020), "Control of specific growth rate in fed-batch bioprocesses: Novel controller design for improved noise management", *Processes*, 8 (6), ISSN: 22279717, DOI: 10.3390/PR8060679.

Butkus, M, Repšyte, J and Galvanauskas, V (Oct. 2020), "Fuzzy logic-based adaptive control of specific growth rate in fed-batch biotechnological processes. A simulation study", *Applied Sciences (Switzerland)*, 10 (19), ISSN: 20763417, DOI: 10.3390/app10196818.

Cepeda, M, Waniska, R, Rooney, L and Bejosano, F (2000), "Effects of leavening acids and dough temperature in wheat flour tortillas", *Cereal Chemistry*, 77 (4): 489–494, ISSN: 00090352, DOI: 10.1094/CCHEM.2000.77.4.489.

Chatterjee, S, Chatterjee, S, Chatterjee, B and Guha, A (2008), "Enhancement of growth and chitosan production by *Rhizopus oryzae* in whey medium by plant growth hormones", *International Journal of Biological Macromolecules*, 42 (2): 120–126, ISSN: 01418130, DOI: 10.1016/j.ijbiomac.2007.10.006.

Chia, DW, Yoder, TJ, Reiter, WD and Gibson, SI (2000), "Fumaric acid: An overlooked form of fixed carbon in Arabidopsis and other plant species", *Planta*, 211 (5): 743–751, ISSN: 00320935, DOI: 10.1007/s004250000345.

Chotisubha-Anandha, N, Thitiprasert, S, Tolieng, V and Thongchul, N (2011), "Improved oxygen transfer and increased l-lactic acid production by morphology control of *Rhizopus oryzae* in a static bed bioreactor", *Bioprocess and Biosystems Engineering*, 34 (2): 163–172, ISSN: 16157591, DOI: 10.1007/s00449-010-0457-z.

Dantigny, P, Guilmart, A, Radoi, F, Bensoussan, M and Zwietering, M (2005), "Modelling the effect of ethanol on growth rate of food spoilage moulds", *International Journal of Food Microbiology*, 98 (3): 261–269, ISSN: 01681605, DOI: 10.1016/j.ijfoodmicro.2004.07.008.

Das, R, Brar, S and Verma, M (2015), "Enhanced fumaric acid production from brewery wastewater by immobilization technique", *Journal of Chemical Technology and Biotechnology*, 90 (8): 1473–1479, ISSN: 10974660, DOI: 10.1002/jctb.4455.

Das, R, Brar, S and Verma, M (2016), "Fumaric Acid", *Platform Chemical Biorefinery*, (June 2016): 133–157, DOI: 10.1016/b978-0-12-802980-0.00008-0.

Deken, R (1966), "The Crabtree effect: A regulatory system in yeast", *Journal of General Microbiology*, (1): 149–156.

Deng, F and Aita, GM (2018), "Fumaric Acid Production by Rhizopus oryzae ATCC® 20344™ from Lignocellulosic Syrup", *Bioenergy Research*, 11 (2): 330–340, ISSN: 19391242, DOI: 10.1007/s12155-018-9899-y.

Doscher, C, Kane, J, Cragwall, G and Staebner, W (1941), "Industrial applications of fumaric acid", *Industrial & Engineering Chemistry*, 33 (3): 315–319, ISSN: 0019-7866, DOI: 10.1021/ie50375a008.

Foster, JW and Waksman, SA (1939), "The Production of Fumaric Acid by Molds Belonging to the Genus Rhizopus", *Journal of the American Chemical Society*, 61 (1): 127–135, ISSN: 15205126, DOI: 10.1021/ja01870a043.

Fu, Y, Xu, Q, Li, S, Chen, Y and Huang, H (2010), "Strain improvement of *Rhizopus oryzae* for over-production of fumaric acid by reducing ethanol synthesis pathway", *Korean Journal of Chemical Engineering*, 27 (1): 183–186, ISSN: 02561115, DOI: 10.1007/s11814-009-0323-3.

Ghosh, B and Rani Ray, R (Dec. 2011), "Current commercial perspective of *Rhizopus oryzae*: A review", *Journal of Applied Sciences*, 11 (14): 2470–2486, ISSN: 18125654, DOI: 10.3923/jas.2011.2470.2486, URL: http://www.scialert.net/abstract/?doi=jas.2011.2470.2486.

Grand View Research (2019), *Maleic Anhydride Market Size, Share & Trends Analysis Report By Application (1,4-BDO, UPR, Additives, Copolymers), By Region (Asia Pacific, North America, Europe, Central & South America, MEA), And Segment Forecasts, 2019 - 2025*, tech. rep.: pp. 1–120, URL: https://www.grandviewresearch.com/industry-analysis/maleic-anhydride-market.

Habegger, L, Crespo, KR and Dabros, M (Sept. 2018), "Preventing overflow metabolism in Crabtree-positive microorganisms through on-line monitoring and control of fed-batch fermentations", *Fermentation*, 4 (3), ISSN: 23115637, DOI: 10.3390/fermentation4030079.

Ilica, RA, Kloetzer, L, Galaction, AI and Caşcaval, D (2019), "Fumaric acid: production and separation", *Biotechnology Letters*, 41 (1): 47–57, ISSN: 15736776, DOI: 10.1007/s10529-018-2628-y.

Lan, R and Kim, I (2018), "Effects of organic acid and medium chain fatty acid blends on the performance of sows and their piglets", *Animal Science Journal*, 89 (12): 1673–1679, ISSN: 17400929, DOI: 10.1111/asj.13111.

Li, X, Yu, C, Yao, J, Wang, Z and Lu, S (2018), "An online respiratory quotient-feedback strategy of feeding yeast extract for efficient arachidonic acid production by Mortierella alpina", *Frontiers in Bioengineering and Biotechnology*, 5 (JAN): 1–11, ISSN: 22964185, DOI: 10.3389/fbioe.2017.00083.

Liao, W, Liu, Y and Chen, S (2007), "Studying pellet formation of a filamentous fungus Rhizopus oryzae to enhance organic acid production", *Applied Biochemistry and Biotechnology*, 137-140 (1-12): 689–701, ISSN: 02732289, DOI: 10.1007/s12010-007-9089-4.

Liao, W, Liu, Y, Frear, C and Chen, S (2008), "Co-production of fumaric acid and chitin from a nitrogen-rich lignocellulosic material - dairy manure - using a pelletized filamentous fungus Rhizopus oryzae ATCC 20344", *Bioresource Technology*, 99 (13): 5859–5866, ISSN: 09608524, DOI: 10.1016/j.biortech.2007.10.006.

Maneeboon, T, Vanichsriratana, W, Pomchaitaward, C and Kitpreechavanich, V (2010), "Optimization of lactic acid production by pellet-form *Rhizopus oryzae* in 3-l airlift bioreactor using response surface methodology", *Applied Biochemistry and Biotechnology*, 161 (1-8): 137–146, ISSN: 02732289, DOI: 10.1007/s12010-009-8860-0.

Mrowietz, U, Christophers, E and Altmeyer, P (1999), "Treatment of severe psoriasis with fumaric acid esters: Scientific background and guidelines for therapeutic use", *British Journal of Dermatology*, 141 (3): 424–429, ISSN: 00070963, DOI: 10.1046/j.1365-2133.1999.03034.x.

Naude, A and Nicol, W (2017), "Fumaric acid fermentation with immobilised *Rhizopus oryzae*: Quantifying time-dependent variations in catabolic flux", *Process Biochemistry*, 56 (March): 8–20, ISSN: 13595113, DOI: 10.1016/j.procbio.2017.02.027, URL: http://dx.doi.org/10.1016/j.procbio.2017.02.027.

Naude, A and Nicol, W (2018a), "Improved continuous fumaric acid production with immobilised *Rhizopus oryzae* by implementation of a revised nitrogen control strategy", *New Biotechnology*, 44 (April): 13–22, ISSN: 18764347, DOI: 10.1016/j.nbt.2018.02.012, URL: https://doi.org/10.1016/j.nbt.2018.02.012.

Naude, A and Nicol, W (2018b), "Malic acid production through the whole-cell hydration of fumaric acid with immobilised *Rhizopus oryzae*", *Biochemical Engineering Journal*, 137: 152–161, ISSN: 1873295X, DOI: 10.1016/j.bej.2018.05.022, URL: https://doi.org/10.1016/j.bej.2018.05.022.

Odoni, DI, Tamayo-Ramos, JA, Sloothaak, J, Heck, RG van, Martins dos Santos, VA, Graaff, LH de, Suarez-Diez, M and Schaap, PJ (2017), "Comparative proteomics of Rhizopus delemar ATCC 20344 unravels the role of amino acid catabolism in fumarate accumulation", *PeerJ*, 2017 (3): 1–18, ISSN: 21678359, DOI: 10.7717/peerj.3133.

Park, E, Kosakai, Y and Okabe, M (1998), "Efficient production of L-(+)-lactic acid using mycelial cotton-like flocs of *Rhizopus oryzae* in an air-lift bioreactor", *Biotechnology Progress*, 14 (5): 699–704, ISSN: 87567938, DOI: 10.1021/bp9800642.

Patten, J and Waldroup, P (1988), "Use of organic acids in broiler diets", *Poultry Science*, 67 (8): 1178–1182, ISSN: 00325791, DOI: 10.3382/ps.0671178.

Rhodes, R, Lagoda, A, Misenheimer, T, Smith, M, Anderson, R and Jackson, R (1962), "Production of fumaric acid in 20-liter fermentors", *Applied Microbiology*, 10 (1): 9–15, ISSN: 0003-6919, DOI: 10.1128/aem.10.1.9-15.1962.

Roa Engel, C, Straathof, A, Zijlmans, T, Van Gulik, W and Van der Wielen, L (2008), "Fumaric acid production by fermentation", *Applied Microbiology and Biotechnology*, 78 (3): 379–389, ISSN: 01757598, DOI: 10.1007/s00253-007-1341-x.

Roa Engel, C, Van Gulik, W, Marang, L, Van der Wielen, L and Straathof, A (2011), "Development of a low pH fermentation strategy for fumaric acid production by *Rhizopus oryzae*", *Enzyme and Microbial Technology*, 48 (1): 39–47, ISSN: 01410229, DOI: 10.1016/j.enzmictec.2010.09.001, URL: http://dx.doi.org/10.1016/j.enzmictec.2010.09.001.

Rokicki, G and Wodzicki, H (2000), "Waterborne unsaturated polyester resins", *Macromolecular Materials and Engineering*, 278: 17–22, ISSN: 14387492, DOI: 10.1002/(SICI)1439-2054(20000501)278:1<17::AID-MAME17>3.0.CO;2-3.

Schimrigk, S, Brune, N, Hellwig, K, Lukas, C, Bellenberg, B, Rieks, M, Hoffmann, V, Pöhlau, D and Przuntek, H (2006), "Oral fumaric acid esters for the treatment of active multiple sclerosis: An open-label, baseline-controlled pilot study", *European Journal of Neurology*, 13 (6): 604–610, ISSN: 13515101, DOI: 10.1111/j.1468-1331.2006.01292.x.

Sebastian, J, Hegde, K, Kumar, P, Rouissi, T and Brar, S (2019), "Bioproduction of fumaric acid: An insight into microbial strain improvement strategies", *Critical Reviews in Biotechnology*, 39 (6): 817–834, ISSN: 15497801, DOI: 10.1080/07388551.2019.1620677, URL: https://doi.org/10.1080/07388551.2019.1620677.

Sepehri, A and Sarrafzadeh, MH (2018), "Effect of nitrifiers community on fouling mitigation and nitrification efficiency in a membrane bioreactor", *Chemical Engineering and Processing - Process Intensification*, 128 (December 2017): 10–18, ISSN: 02552701, DOI: 10.1016/j.cep.2018.04.006.

Sepehri, A, Sarrafzadeh, MH and Avateffazeli, M (2020), "Interaction between Chlorella vulgaris and nitrifying-enriched activated sludge in the treatment of wastewater with low C/N ratio", *Journal of Cleaner Production*, 247, ISSN: 09596526, DOI: 10.1016/j.jclepro.2019.119164.

Shukla, P (2017), "Food additives from an organic chemistry perspective", *MOJ Bioorganic & Organic Chemistry*, 1 (3): 70–79, DOI: 10.15406/mojboc.2017.01.00015.

Song, C, Kim, D, Choi, S, Jang, J and Lee, S (2013), "Metabolic engineering of *Escherichia coli* for the production of fumaric acid", *Biotechnology and Bioengineering*, 110 (7): 2025–2034, ISSN: 00063592, DOI: 10.1002/bit.24868.

Swart, R, le Roux, F, Naude, A, de Jongh, N and Nicol, W (2020), "Fumarate production with *Rhizopus oryzae*: Utilising the Crabtree effect to minimise ethanol by-product formation", *Biotechnology for Biofuels*, 13 (1): 1–10, ISSN: 17546834, DOI: 10.1186/s13068-020-1664-8, URL: https://doi.org/10.1186/s13068-020-1664-8.

Venkataramaniah, M and Raghava Rao, BS (1951), "Estimation and separation of zirconium by use of fumaric acid", *The Analyst*, 76 (899): 107–109, ISSN: 00032654, DOI: 10.1039/an9517600107.

Wang, Z, Wang, Y, Yang, S, Wang, R and Ren, H (2010), "A novel honeycomb matrix for cell immobilization to enhance lactic acid production by *Rhizopus oryzae*", *Bioresource Technology*, 101 (14): 5557–5564, ISSN: 09608524, DOI: 10.1016/j.biortech.2010.02.064, URL: http://dx.doi.org/10.1016/j.biortech.2010.02.064.

Werpy, T and Petersen, G (2004), *Top Value Added Chemicals from Biomass Volume I*, tech. rep.: Medium: ED, Size: 76 pp. pages, DOI: 10.2172/15008859, URL: http://www.osti.gov/scitech//servlets/purl/15008859-s6ri0N/native/.

Woehrer, W and Roehr, M (1981), "Regulatory aspects of bakers' yeast metabolism in aerobic fed-batch cultures", *Biotechnology and Bioengineering*, 23 (3): 567–581, ISSN: 10970290, DOI: 10.1002/bit.260230308.

Wojcieszak, R, Santarelli, F, Paul, S, Dumeignil, F, Cavani, F and Gonçalves, RV (2015), "Recent developments in maleic acid synthesis from bio-based chemicals", *Sustainable Chemical Processes*, 3 (1): 1–11, ISSN: 2043-7129, DOI: 10.1186/s40508-015-0034-5.

Yin, P, Yahiro, K, Ishigaki, T, Park, Y and Okabe, M (1998), "L(+)-lactic acid production by repeated batch culture of *Rhizopus oryzae* in air-lift bioreactor", *Journal of Fermentation and Bioengineering*, 85 (1): 96–100, ISSN: 0922338X, DOI: 10.1016/S0922-338X(97)80361-3.

Zhang, B, Skory, C and Yang, S (2012), "Metabolic engineering of *Rhizopus oryzae*: Effects of overexpressing pyc and pepc genes on fumaric acid biosynthesis from glucose", *Metabolic Engineering*, 14 (5): 512–520, ISSN: 10967176, DOI: 10.1016/j.ymben.2012.07.001, URL: http://dx.doi.org/10.1016/j.ymben.2012.07.001.

Zhang, B and Yang, S (2012), "Metabolic engineering of *Rhizopus oryzae*: Effects of overexpressing fumR gene on cell growth and fumaric acid biosynthesis from glucose", *Process Biochemistry*, 47 (12): 2159–2165, ISSN: 13595113, DOI: 10.1016/j.procbio.2012.08.009, URL: http://dx.doi.org/10.1016/j.procbio.2012.08.009.

Zhang, XC, Visala, A, Halme, A and Linko, P (1994), "Functional state modelling approach for bioprocesses: Local models for aerobic yeast growth processes", *Journal of Process Control*, 4 (3): 127–134, ISSN: 09591524, DOI: 10.1016/0959-1524(94)85004-6.

Zhou, Y, Du, J and Tsao, G (2000), "Mycelial pellet formation by *Rhizopus oryzae* ATCC 20344", *Applied Biochemistry and Biotechnology - Part A Enzyme Engineering and Biotechnology*, 84-86: 779–789, ISSN: 02732289, DOI: 10.1385/abab:84-86:1-9:779.